

DOMAIN WALLS IN THE QUANTUM TRANSVERSE ISING MODEL

Malte Henkel,¹ A. Brooks Harris,^{1,2} and Marek Cieplak³

(1) *Theoretical Physics, Oxford University, 1 Keble Rd. Oxford OX1 3NP, UK*

(2) *Department of Physics, University of Pennsylvania, Philadelphia, PA 19104-6396*

(3) *Institute of Physics, Polish Academy of Sciences, 02-668 Warsaw, Poland*

(September 17, 2018)

Abstract

We discuss several problems concerning domain walls in the spin S Ising model at zero temperature in a magnetic field, $H/(2S)$, applied in the x direction. Some results are also given for the planar (y - z) model in a transverse field. We treat the quantum problem in one dimension by perturbation theory at small H and numerically over a large range of H . We obtain the spin density profile by fixing the spins at opposite ends of the chain to have opposite signs of S_z . One dimension is special in that there the quantum width of the wall is proportional to the size L of the system. We also study the quantitative features of the ‘particle’ band which extends up to energies of order H above the ground state. Except for the planar limit, this particle band is well separated from excitations having energy J/S involving creation of more walls. At large S this particle band develops energy gaps and the lowest sub-band has tunnel splittings of order $H2^{1-2S}$. This scale of energy gives rise to anomalous scaling with respect to a) finite size, b) temperature, or c) random potentials. The intrinsic width of the domain wall and the pinning energy are also defined and calculated in certain limiting cases. The general conclusion is that quantum effects prevent the wall from being sharp and in

higher dimension would prevent sudden excursions in the configuration of the wall.

PACS numbers: 75.30.Et, 71.70.Ej, 75.30.Gw, 75.10.N, 75.10.H

I. INTRODUCTION

Recently, there has been a growing interest in the study of interfaces with non-trivial geometry. Such interfaces arise in a variety of situations including domain walls in random magnets,^{1,2,3,4,5,6} fluid invasion in porous media^{1,7}, spreading on heterogeneous surfaces⁸, membranes and vesicles in biology,⁹ and epitaxial growth in materials science.^{1,10}

In connection with such problems it is natural to ask whether quantum effects play a significant role. For static properties it is well established that in nonrandom systems, such as a spin S antiferromagnet, with only a nearest neighbor exchange interaction, J , there are various regimes. Near the critical temperature at $T_N \sim JS^2$, thermal fluctuations are dominant. In the ordered phase, as long as $T_c/S \ll T \ll T_c$, quantum effects due to the finiteness of S are unimportant. For $T < T_c/S$ one is in a quantum regime, where the quantum statistics of spin waves and their interactions leads to dependences on S and T not present in the classical ($S \rightarrow \infty$) limit. Heuristic arguments indicate that quantum effects could influence the nature of domain walls in spin systems. In the picture in which the trajectory of the domain wall is likened to the trajectory of a particle in space as a function of time, quantum effects cause a smearing out of the trajectory. For such a system analytic and numerical work is obviously very difficult. Accordingly, we have been led to carry out a program of analytic work for quantum domain walls in one dimension. For this purpose we consider domain walls at zero temperature T in the spin S Ising model (with nearest-neighbor exchange coupling J) in a transverse field, H , whose Hamiltonian is

$$\mathcal{H}_{TI} = -\frac{H}{2S} \sum_n S_x(n) - \frac{J}{2S^2} \sum_n S_z(n) S_z(n+1) , \quad (1)$$

where $\mathbf{S}(n)$ is a quantum spin S operator at site n .

To study domain walls in this model we introduce boundary conditions in which the spin at one end of the chain is fixed to be “up” and that at the other end is fixed to be “down.” This model has some interest in its own right. For $S = 1/2$ its properties can, in principle, be related to those of the associated free Fermion model obtained via the Jordan-Wigner¹¹ transformation. However, with domain-wall boundary conditions, this relation is

not easy to implement. Accordingly, we approach the analysis of the properties of domain walls in this model via perturbation theory for $H/J \ll 1$ and more generally via numerical solution for the wave functions and energies of the ground state and the low-lying excited states. Needless to say, some of the properties of this model in one dimension can not be extrapolated to higher dimensional systems. However, in most cases, one can safely say which features can be so extrapolated and which can not.

We may summarize our results for the one dimensional model as follows. The magnetization profile has a width of order the length of the chain. The low-lying excited states comprise a manifold of “particle” states, which results when the center of the wall propagates from site to site. These results are easily understood within perturbation theory in H/J . In the classical limit the width of the wall is of order the correlation length, i. e. it is of order a lattice constant, as long as one is far from the critical regime at $H \approx 2J$, above which long range order disappears. In the classical limit and for small H/J , we evaluate a barrier energy, analogous to the Peierls-Nabarro energy,¹² which prevents the free motion of the domain wall. When the correlation length becomes very large this barrier energy becomes small and since it is harder to calculate in this limit, we did not attempt such calculations. It would be interesting to calculate this energy for a quantum system, but in the present case, since the width of the wall is of order L , we can say that this barrier energy vanishes in the thermodynamic limit. Also, in the large S limit, we find that the quantum hopping of the domain wall from one site to the next is actually analogous to a tunneling process, so that the hopping matrix element is not of order H , as it is for the low spin case, but is now of order $H \exp(-aS)$, where $a = \ln 2$. It would be of some interest to recover this result within a field theory of one space and one time dimension to describe such a quantum effect.

Briefly, this paper is organized as follows. In Sec. II we define the class of models we will analyze in one dimension. In Sec. III we give numerical results for the magnetization profile for $S = 1/2$, $S = 1$ and $S = 3/2$ and compare these to analytic results we obtain using perturbation theory in the small H/J limit. In Sec. IV we give analytic results for large S . The classical results for $S = \infty$ are given both in the continuum limit (i.e., when the wall is

very broad) and in the discrete limit (when the wall is very narrow). Here we also analyze the quantum system for large S . In Sec. V we give various results concerning the nature of the energy spectrum in the presence of a domain wall. We give numerical and analytic results for the nature of the particle spectrum caused by the matrix element which allows the wall to hop from one site to the next. Finally, in Sec. VI we summarize the conclusions to be drawn from our work.

II. DEFINITION OF ONE DIMENSIONAL MODELS

The first one-dimensional model we consider is the spin S Ising model in a transverse field, with the Hamiltonian

$$\mathcal{H}_{\text{TI}} = -\frac{H}{2S} \sum_{n=1}^L S_x(n) - \frac{J}{2S^2} \sum_{n=0}^L S_z(n) S_z(n+1) . \quad (2)$$

This formulation of the model has the advantages that a) the domain wall energy (for $H = 0$) is independent of the value of S and is equal to J , and b) the mean-field transition temperature T_0 (at which significant correlations begin to develop between neighboring spins) is of order J independent of S . To discuss domain walls, the spins $S(0)$ and $S(L+1)$ will be fixed by boundary conditions, as discussed below. Thus L is the number of “active” spins in the chain. We will often use the notation $h = H/J$.

We will also consider the “yz” model in a transverse field, for which the Hamiltonian is

$$\mathcal{H}_{\text{yz}} = -\frac{H}{2S} \sum_{n=1}^L S_x(n) - \frac{J}{2S^2} \sum_{n=0}^L \left(S_z(n) S_z(n+1) + \epsilon S_y(n) S_y(n+1) \right) . \quad (3)$$

The most important difference between these two models is that the interaction term (proportional to ϵ) in \mathcal{H}_{yz} allows the spins to tip away from the z -axis. For $H = 0$ and with free-end boundary conditions, the “y-z” model with $\epsilon = 1$ has the continuous $U(1)$ symmetry instead of the discrete Z_2 symmetry of the Ising model which results when $\epsilon \neq 1$. In fact, we recall the ground state phase diagram¹¹ of this more general model, shown in Fig. 1 for spin $S = \frac{1}{2}$, where one sees (at zero temperature) the disordered phase (D), the ordered

ferromagnetic Ising phase (F), and the ordered oscillatory phase (O). In both ordered phases the spontaneous magnetization $\langle S_z(n) \rangle$ is non-vanishing (where $\langle \dots \rangle$ denotes the thermodynamic average at temperature T). However, the (connected) two-point correlation function, $G(R) = \langle S_z(R)S_z(0) \rangle - \langle S_z(R) \rangle \langle S_z(0) \rangle$, behaves as follows¹¹ for $R \rightarrow \infty$:

$$G(R) \sim \begin{cases} R^{-1/2} \exp(-R/\xi), & \text{phase D;} \\ R^{-2} \exp(-R/\xi), & \text{phase F;} \\ R^{-2} \exp(-2R/\xi) \cdot \text{Re} B e^{iKR}, & \text{phase O;} \end{cases} \quad (4)$$

where the correlation length ξ is a known function of h and ϵ in each of the three phases, B is a constant and $\cos K = \sqrt{h^2/(4\epsilon)}$. When going from phase F to phase O, there is a new diverging length $\Lambda \sim 1/K$, which is not simply related to a gap in the spectrum of \mathcal{H}_{yz} (as is ξ), but indicates the wavelength at which the correlation function at large distances oscillates under an exponentially decaying envelope.

To discuss the width and energy of a domain wall, we shall work with “up-down” boundary conditions, in which we require

$$S_z(0) = -S_z(L+1) = S. \quad (5)$$

We can then study the profile of the wall by evaluating

$$M(n) = \langle 0 | S_z(n) | 0 \rangle / S, \quad (6)$$

where $|0\rangle$ denotes the ground state. As we discuss in more detail below, in order to obtain a spin profile for a *quantum* system, antiperiodic boundary conditions which introduce a boundary coupling $(K/2)S_z(0)S_z(L+1)$ *cannot* be used in a naive way. However, for a classical system such antiperiodic boundary conditions will prove convenient. The energy of the domain wall, E_w , is defined to be $E_w = E - E_p$, where E is the energy with “up-down” or antiperiodic boundary conditions and E_p that with “up-up” or periodic boundary conditions.

III. RESULTS FOR THE PROFILE FUNCTION FOR $S = 1/2, 1$ AND $3/2$

A. Numerical Results for the Ferromagnetic Phase

We begin by presenting numerical results for the profile function $M(n)$ for the ferromagnetic phase F. For general spin we are constrained to rather small systems, since the number of quantum states is $(2S + 1)^L$ for L sites (excluding the fixed boundary spins). So why not use translational symmetry to reduce the number of states?

Indeed, that would be possible for the special case of antiperiodic boundary conditions (with $K = J$) mentioned in the previous section. These boundary conditions are peculiar since \mathcal{H} commutes with the modified translation operator $\tilde{\mathcal{T}} = \sigma_x(0)\mathcal{T}$ where \mathcal{T} is the usual translation operator and $\sigma_x(0)$ changes the sign of $\sigma_z(0)$. In addition, \mathcal{H} can be decomposed (for any K) into a block diagonal form. The corresponding states are said to be in the even or odd sector, respectively, depending on their parity under spin reversal. Furthermore, $M(n) = 0$ in that case and one should consider instead the quantity $\tilde{M}(n) = \langle 0|S_z(n)|1\rangle$ where $|0\rangle$ and $|1\rangle$ are the ground states in the even and odd sectors (with respect to the Ising symmetry) of the model, respectively. It is well-known that at least for *periodic* boundary conditions this defines¹³ a sensible finite-lattice approximation to the order parameter (see Ref. 14 and references therein). However, for $K = J$, even for L finite, there are two *degenerate* states $|1\rangle, |1'\rangle$ in the odd sector, one of which gives rise to the desired wall profile, while the profile of the other one is essentially flat. On the other hand, for $K > J$, one does get a wall profile, but its shape depends on the value of K/J . We avoid these problems by choosing the “up-down” boundary conditions defined above in Eq. (5). Furthermore, since we are interested in situations far from criticality, the convergence of the finite-size data with $L \rightarrow \infty$ is usually quite rapid so that the moderate sizes achieved are sufficient for our purposes.

The determination of the lowest eigenstates of the Hamiltonians \mathcal{H}_{TI} and \mathcal{H}_{yz} using the Lanczos algorithm is fairly standard¹⁴. From the ground state $|0\rangle$ we calculate the local

magnetization $m(r)$

$$m(r) = \langle 0 | S_z(n) / S | 0 \rangle \quad , \quad r = n / (L + 1) \quad . \quad (7)$$

Our results pertaining to the ferromagnetic phase F are as follows. In Fig. 2, we display $m(r)$ for $h = 0.1$ and $\epsilon = 0$ and $S = \frac{1}{2}$ for various values of L . With the exception of the smallest L -values used, we first observe that the data collapse onto a single curve, which implies that the L considered are already sufficiently large as compared to the correlation length that they represent the $L \rightarrow \infty$ limit. Second, we note that the profile is quite wide and a continuous function of r . We find a similar data collapse for all the situations we are going to consider in the sequel. Next, we show in Fig. 3, that the overall shape of the profile is not a peculiarity of having spin $S = \frac{1}{2}$. Rather, we see that the profiles obtained with the parameters $\epsilon = 0$ and $h = 0.1$ (Fig. 3A) and $h = 0.5$ (Fig. 3B) both spins $S = 1$ and $S = \frac{3}{2}$ are very close to the one for $S = \frac{1}{2}$. Nevertheless, the finer details of the respective shapes become different as H increases. Finally, in Fig. 4, we show the effect of varying h in the $S = \frac{1}{2}$ case. Note that the profiles for a transverse field as small as $h = 10^{-5}$ and as large as $h = 0.1$ are superimposed onto each other. The fact that the width w of the domain wall is proportional to the size of the system is a peculiarity of a one dimensional quantum model. In higher dimensions we would expect w to remain finite as $L \rightarrow \infty$ except possibly at a critical point where the correlation length diverges.

We shall turn to a quantitative explanation of these findings below. Profiles for the oscillatory phase are discussed in subsection C.

B. Simplified Calculations for the Small S Quantum Case

In order to gain some understanding of the results of the last section, we now present some simple approximate calculations. As it turns out, most of the physics of the problem for h small is conveniently described in terms of degenerate perturbation theory involving the manifold \mathcal{M} of the $h = 0$ ground states. This procedure avoids the additional technical

complications of the free fermion method for “up-down” boundary conditions. The boundary conditions are that spin $S(0)$ is fixed to have $S_z = S$ and spin $S(L+1)$ has $S_z = -S$. For $S = 1/2$ the manifold \mathcal{M} contains the states $|n\rangle$, for $n = 1, 2, \dots, L+1$, where $|n\rangle$ denotes the quantum state (shown in Fig. 5) in which spins i with $i < n$ have their z -component of spin equal to $+1/2$ and those with $i \geq n$ have their z -component of spin equal to $-1/2$. The only nonzero matrix elements of the Hamiltonian within the ground manifold are

$$\begin{aligned}\mathcal{H}_{n,n} &= E_0 \equiv -\frac{1}{2}(L-1)J, \quad 1 \leq n \leq L+1; \\ \mathcal{H}_{n,n+1} &= \mathcal{H}_{n+1,n} = \frac{1}{2}H, \quad 1 \leq n \leq L.\end{aligned}\tag{8}$$

Considering only the manifold \mathcal{M} , one finds the corresponding eigenvectors ψ_p , and eigenenergies E_p (for $p = 1, 2, \dots, L+1$) to be

$$\psi_p = C \sum_{n=1}^{L+1} \sin[np\pi/(L+2)]|n\rangle, \quad E_p = E_0 + H \cos[p\pi/(L+2)], \tag{9}$$

where C is a normalization constant. Perturbative corrections to the energy will occur at order H^2/J and to the wavefunction at order H/J . We may calculate the profile function within the small h approximation:

$$\begin{aligned}M_p(n) &\equiv \psi_p^\dagger (S_{nz}/S) \psi_p = \frac{\sum_{k=n+1}^{L+1} \sin^2[kp\pi/(L+2)] - \sum_{k=1}^n \sin^2[kp\pi/(L+2)]}{\sum_{k=1}^{L+1} \sin^2[kp\pi/(L+2)]} \\ &= 1 - 2 \frac{\sum_{k=1}^n \sin^2[kp\pi/(L+2)]}{\sum_{k=1}^{L+1} \sin^2[kp\pi/(L+2)]} \\ &= 1 - 2 \frac{(2n+1) \sin \frac{p\pi}{L+2} - \sin \frac{(2n+1)p\pi}{L+2}}{(2L+3) \sin \frac{p\pi}{L+2} - \sin \frac{(2L+3)p\pi}{L+2}}.\end{aligned}\tag{10}$$

We set $n = xL$ and work in the limit of infinite L . Thereby we find

$$m_p(x) \equiv M_p(xL) = 1 - 2x + \frac{1}{p\pi} \sin(2px\pi). \tag{11}$$

In Fig. 3, $m_1(r)$ is shown together with the numerically determined ground-state profiles $m(r)$ for $S = \frac{1}{2}$, $S = 1$ and $S = \frac{3}{2}$ and we find a nice qualitative agreement (even for moderately large values of h).

The above calculation can be generalized to larger S . Consider a state in which the wall is between lattice sites. In this state let all spins to the left of the wall have $S_z = S$ and

those to the right have $S_z = -S$. Note that it is possible to change the value of S_z for *either one* (but not simultaneously both) of the spins adjacent to the wall without changing the unperturbed ($h = 0$) energy. For spin $S = 1$ since the nonzero matrix elements of the perturbation due to the transverse field are all the same, the problem is totally equivalent to a spin $1/2$ chain of twice the length. This observation explains the fact that our results for $S = 1/2$ and $S = 1$ are indistinguishable. When $S > 1$, one has to account for the fact that to move the wall through one lattice constant involves matrix elements which depend on the initial and final values of S_z . This case will be considered later.

C. Profile Function for the Oscillatory Phase

The discussion has been so far restricted to the ferromagnetic phase F. The oscillatory phase is distinguished from it by showing a non-monotonic decrease of the correlation function [see Eq. (4)]. How does this behavior manifest itself on the level of the magnetization profile $m(r)$?

To answer this question, we display in Fig. 6A, for $S = \frac{1}{2}$, $m(r)$ for $h = 0.01$ and $\epsilon = 0.5$ and for L even. Indeed, this profile is distinct from the ones observed previously in the phase F. First, finite-size effects are much larger than in the situations discussed before. Second, $m(r)$ displays, at least for L finite, a step-like behavior and it looks as if the system was built out of hard objects each occupying two lattice sites. When h is increased, these composites soften until they completely melt at the transition towards the F phase.

This picture is modified in interesting ways for L odd. In fact, the calculation of $m(r)$ requires a little more care in this case. For L even, the system has a single well-defined ground state separated by a gap at least of order $\mathcal{O}(L^{-3})$ (see Sec. V) from the excited states. That is not so for L odd. Rather, for $h = 0$ but $\epsilon \neq 0$, one finds that the ground state is twofold degenerate. That is a new degeneracy which has nothing to do with the ferromagnetic ordering of the system. Even when $h \neq 0$, the two lowest states in \mathcal{M} remain much closer to each other than with the other states, the latter one having gaps of order

$\mathcal{O}(L^{-2})$. This new (near) degeneracy implies that one must reconsider the calculation of the magnetization profile $m(r)$. Rather than blindly using Eq. (7), we take the *two* ground states $|0\rangle$ and $|0'\rangle$ to be nearly degenerate. Then we construct the matrix

$$\mathbf{m}(r) = S^{-1} \begin{pmatrix} \langle 0|S_z(n)|0\rangle & \langle 0'|S_z(n)|0\rangle \\ \langle 0|S_z(n)|0'\rangle & \langle 0'|S_z(n)|0'\rangle \end{pmatrix}, \quad r = n/(L+1) \quad (12)$$

and find its two eigenvalues $m_{\pm}(r)$. Each of those represents a magnetization profile and one of them is shown in Fig. 6B. The other profile is obtained by reflection around $r = 0.5$. The asymmetry in Fig. 6B, observed for L odd and finite, is easily understood in terms of the composite objects introduced above. Note that within the manifold \mathcal{M} , the $y - y$ term in the Hamiltonian moves the wall through two lattice spaces. Since we are discussing $h = 0$, this is the only kinetic energy of the domain wall. Thus, if we write $\mathcal{M} = \mathcal{M}_e + \mathcal{M}_o$, where \mathcal{M}_e (\mathcal{M}_o) is the submanifold of state in which there are an even (odd) number of up spins, then there are no matrix elements between these two submanifolds. Furthermore, these two submanifolds are related to one another by spatial inversion (accompanied by $S_z \rightarrow -S_z$). Thus, for L odd, the problem decomposes into two identical eigenvalue problems (hence the twofold degeneracy of the energies). The matrix to be diagonalized is exactly the one considered in Sec. III.B, but now for $M = (L+1)/2$ sites and with $h \rightarrow -\epsilon$. The two sets of eigenstates are thus

$$\begin{aligned} \psi_p^{(-)} &= C \sum_{m=1}^M \sin\left(\frac{2\pi pm}{L+3}\right) |2m-1\rangle \\ \psi_p^{(+)} &= C \sum_{m=1}^M \sin\left(\frac{2\pi pm}{L+3}\right) |2m\rangle, \end{aligned} \quad (13)$$

where C is a normalization constant. This eigenvector basis also renders the matrix (12) diagonal. Writing $n = 2k-1$ and $n = 2k$, respectively, we find for the profile for the $+$ set of eigenstates (indicated by a subscript “+”)

$$M_p^+(2k-1) = M_p^+(2k) = 1 - 2 \frac{(2k+1) \sin(2\pi p/(L+3)) - \sin((2k+1)2\pi p/(L+3))}{(L+2) \sin(2\pi p/(L+3)) - \sin((L+2)2\pi p/(L+3))}. \quad (14)$$

In particular, this reproduces the steps in $m_1^+(r)$ observed numerically. Now, taking the continuum limit, it is easy to see that the width of the terraces decreases as $L \rightarrow \infty$ and that $\tilde{m}(x) \rightarrow m(x) + \mathcal{O}(1/L)$. We therefore suggest that the phenomenon observed in Fig. 7 is a novel type of finite-size effect. As $L \rightarrow \infty$, the step-like and asymmetric profiles found for L finite will converge towards a smooth and symmetric limit function.

At least for $h \rightarrow 0$, this limit function appears to show a simple relationship with the profiles previously found in the F phase. Indeed, our data suggest the following. The profiles for L large as found for $h = 0, \epsilon \neq 0$ are very close to those obtained for $h = h_{\text{eff}}(\epsilon), \epsilon = 0$. For small ϵ our analytic work shows this to be true with $h_{\text{eff}}(\epsilon) = \epsilon$. For larger ϵ we have the phenomenological result,

$$h_{\text{eff}}(\epsilon) \simeq \sqrt{\epsilon} \quad (15)$$

Evidence for this is provided in Fig. 7, where some profiles found for $h = 0$ and $\epsilon \neq 0$ (data points) are collapsed with profiles calculated with $h = h_{\text{eff}}(\epsilon)$.

IV. PROFILES AT LARGE S

In this section we obtain several analytic results in the large S limit. We first analyze the classical ($S \rightarrow \infty$) system. Then we treat the quantum system with S large, but not infinite.

To treat the classical ($S = \infty$) system, we write

$$S_x(n)/S = \cos \phi_n, \quad S_z(n)/S = \sin \phi_n, \quad (16)$$

where ϕ is a continuous classical variable. Then the energy of the classical system is

$$E = -\frac{1}{2}H \sum_{n=1}^L \cos \phi_n - \frac{1}{2}J \sum_{n=1}^{L-1} \sin \phi_n \sin \phi_{n+1}. \quad (17)$$

For the classical calculation without a wall, we will adopt periodic boundary conditions, so that $\phi_{L+1} = \phi_1$ and the last term in Eq. (17) runs from $n = 1$ to $n = L$. In that case $\phi_i = \phi_{\text{eq}} \equiv \arccos \tilde{h}$, where, for convenience, we set

$$H/(2J) = h/2 = h/h_c = \tilde{h} , \quad (18)$$

where $h_c = 2$ is the critical value of h above which long-range Ising order disappears. For the periodic chain the energy per spin, e_0 , is given by

$$e_0 = -\frac{1}{2}J(1 + \tilde{h}^2) . \quad (19)$$

In the classical calculations we will use two types of boundary conditions to generate a wall. The first type of boundary condition is used for the continuum calculation. Here the number of sites is infinite and hence we set $\phi(x = -\infty) = -\phi(\infty) = \phi_{\text{eq}}$. This continuum calculation is valid when the angle ϕ changes slowly with position, as it does for $\tilde{h} \approx 1$. The second type of boundary condition is that used in the discrete calculation. Here it is convenient to use antiperiodic boundary conditions in which spins at opposite ends of the chain are coupled antiferromagnetically, with $K = J$ and we require $\phi_{-i} = -\phi_i$.

In any case, the ground state energy is found by minimizing E with respect to the ϕ 's. Apart from end effects this minimization yields the following conditions (for $n = 2, 3, 4, \dots, N-1$) which characterize the exact ground state,

$$\frac{1}{2} \left(\sin \phi_{n+1} + \sin \phi_{n-1} \right) = (H/2J) \tan \phi_n \equiv \tilde{h} \tan \phi_n . \quad (20)$$

A. Classical Continuum Limit

For small \tilde{h} the angle ϕ will change abruptly at the domain wall and we will treat this case in the next subsection. As \tilde{h} increases (up to the critical value $\tilde{h} = 1$), ϕ_n will become a smoother function of n . In that case, a continuum approximation for ϕ_n makes sense. To treat the continuum limit for $\tilde{h} \approx 1$, we set $\sin \phi_n = y(x) \equiv \sin \phi(x)$, where $x = na$, whence Eq. (20) becomes

$$\tilde{h}y(x) = \frac{1}{2}\sqrt{1 - y(x)^2}[y(x-a) + y(x+a)] . \quad (21)$$

The continuum limit of this equation is

$$\tilde{h}y(x) = \sqrt{1 - y(x)^2} \left[y(x) + \frac{1}{2}a^2 \frac{d^2y}{dx^2} \right]. \quad (22)$$

The solution to this differential equation is reduced to quadratures:

$$\frac{\sqrt{2}x}{a} = \phi(x) + \tilde{h} \frac{1}{\sqrt{1 - \tilde{h}^2}} \ln \left(\frac{1 - \tilde{h} \cos \phi(x) + \sqrt{1 - \tilde{h}^2} \sin \phi(x)}{\cos \phi(x) - \tilde{h}} \right). \quad (23)$$

We now discuss the significance of this result. First we analyze the behavior for large x . At large $|x|$, $\phi(x)$ approaches $\pm\phi_{\text{eq}}$, where $\cos \phi_{\text{eq}} = h$. Thus for large $|x|$ we set $\phi(x) = \pm[\phi_{\text{eq}} - \delta(x)]$. Keeping only the dominant terms in Eq. (23), we obtain

$$\frac{\sqrt{2}x}{a} - \phi_{\text{eq}}(x) = -\frac{\tilde{h}}{\sqrt{1 - \tilde{h}^2}} \ln \left(\frac{\delta(x)}{2(1 - \tilde{h}^2)} \right). \quad (24)$$

This gives

$$\delta(x) = \delta_0 e^{-x/\xi}, \quad (25)$$

where

$$\delta_0 = 2(1 - \tilde{h}^2) \exp \left(a \arccos \tilde{h} / (\sqrt{2}\xi) \right) \quad (26)$$

and ξ is the correlation length, given by

$$\frac{\xi}{a} = \frac{\tilde{h}}{\sqrt{2}\sqrt{1 - \tilde{h}^2}}. \quad (27)$$

Thus, for $\tilde{h} \rightarrow 1$,

$$\xi/a \sim A_\xi (\tilde{h}_c - \tilde{h})^{-\nu}, \quad (28)$$

with $\nu = 1/2$, $\tilde{h}_c = 1$, and $A_\xi = 1/2$.

Next let us see the behavior of the solution near $x = 0$. To do that, differentiate the solution above with respect to x at $x = 0$:

$$\frac{\sqrt{2}}{a} = \frac{d\phi}{dx} + \frac{\tilde{h}}{1 - \tilde{h}} \frac{d\phi}{dx}, \quad (29)$$

where we used $\phi(0) = 0$. This gives

$$\left. \frac{d\phi}{dx} \right]_{x=0} = \frac{\sqrt{2}}{a}(1 - \tilde{h}) . \quad (30)$$

To estimate the width, W , of the wall, we note that over a distance W , the angle ϕ varies from approximately $-\phi_{\text{eq}}$ to approximately $+\phi_{\text{eq}}$. This reasoning indicates that

$$W \left. \frac{d\phi}{dx} \right]_{x=0} = 2\phi_{\text{eq}} , \quad (31)$$

For $h \rightarrow 1$, we have $\phi_{\text{eq}} \approx \sqrt{2}\sqrt{1 - \tilde{h}}$, so that

$$W \approx 2a(1 - \tilde{h})^{-1/2} \approx 4\xi . \quad (32)$$

Thus for $h \rightarrow \tilde{h}_c$, W is of order ξ , as one might expect.

B. Classical Wall At a Lattice Site

In this and the next subsection we look at the discrete equations, which are the appropriate ones for small \tilde{h} . Since we are dealing with a classical system, it is convenient to use antiperiodic boundary conditions in which spins at opposite ends of the chain are coupled antiferromagnetically, with $K = J$.

First we consider the case when the center of the wall is at a lattice site. To treat this case, we consider a chain with an odd number of spins. Number the sites $-N, -N + 1, \dots, -1, 0, 1, \dots, N - 1, N$ and fix $\phi_0 = 0$. Then $\phi_{-n} = -\phi_n$ and the energy E' for this chain of $2N + 1$ sites is

$$E' = -J \sum_{n=1}^{N-1} \sin \phi_n \sin \phi_{n+1} - \frac{1}{2} J \sin^2 \phi_N - H \sum_{n=1}^N \cos \phi_n - \frac{1}{2} H . \quad (33)$$

The ϕ_n are determined by Eq. (20) for $n = 2, 3, \dots, N - 1$, by

$$\frac{1}{2} \sin \phi_2 - \tilde{h} \tan \phi_1 = 0 , \quad (34)$$

and by

$$\frac{1}{2} \sin \phi_{N-1} + \frac{1}{2} \sin \phi_N - \tilde{h} \tan \phi_N = 0 . \quad (35)$$

To obtain the solutions for the ϕ 's at small h we write $\phi_n = \pi/2 - \epsilon_n$ for $\epsilon_n \ll 1$. Then for $1 < j < N$

$$\tilde{h} \cot \epsilon_1 = \frac{1}{2} \cos \epsilon_2 , \quad \tilde{h} \cot \epsilon_j = \frac{1}{2} [\cos \epsilon_{j-1} + \cos \epsilon_{j+1}] , \quad \tilde{h} \cot \epsilon_N = \frac{1}{2} [\cos \epsilon_{N-1} + \cos \epsilon_N] . \quad (36)$$

To obtain the energy at order \tilde{h} we only need to solve the equations correct to order \tilde{h} , in which case

$$\epsilon_1 = 2\tilde{h} , \quad \epsilon_2 = \epsilon_3 \dots = \epsilon_N = \tilde{h} . \quad (37)$$

Then, to find the energy to order \tilde{h} , we may set $\sin \phi_j = 1$, and $\cos \phi_j = (1 + \delta_{j,1})\tilde{h}$, so that

$$-E'/J = (N-1) + \frac{1}{2} + \tilde{h} + O(\tilde{h}^2) . \quad (38)$$

The wall energy E'_w is given by the large N limit of

$$E'_w = E' - (2N+1)e_0 , \quad (39)$$

where e_0 is the energy per site of the uniform chain. Thus

$$E'_w/J = -(N - \frac{1}{2}) - \tilde{h} + (N + \frac{1}{2}) + O(\tilde{h}^2) = 1 - \tilde{h} + O(\tilde{h}^2) . \quad (40)$$

C. Classical Wall Between Lattice Sites

To treat the case when the center of the wall is midway between two lattice sites, we consider a chain of $2N$ sites, numbered $-N, -N+1, \dots, -2, -1, 1, 2, \dots, N-1, N$. We require that $\phi_{-n} = -\phi_n$ and we use the same antiperiodic boundary conditions as in the previous case. Then the energy is

$$E'' = -J \sum_{n=1}^{N-1} \sin \phi_n \sin \phi_{n+1} + \frac{1}{2} J \sin^2 \phi_1 - \frac{1}{2} J \sin^2 \phi_N - H \sum_{n=1}^N \cos \phi_n . \quad (41)$$

As before, the wall energy, E''_w is obtained via

$$E_w'' = E'' - 2Ne_0 . \quad (42)$$

The ϕ_n are determined by Eq. (20) for $n = 2, 3, \dots, N-1$, by Eq. (35), and by

$$\frac{1}{2}(\sin \phi_2 - \sin \phi_1) = \tilde{h} \tan \phi_1 . \quad (43)$$

To analyze these equations, set $\phi_n = \phi_{\text{eq}} - \epsilon_n$. Then, to first order in ϵ_n we have (for $1 < n < N$)

$$\tilde{h} \tan \phi_{\text{eq}} - \frac{\tilde{h}}{\cos^2 \phi_{\text{eq}}} \epsilon_n = \sin \phi_{\text{eq}} - \frac{1}{2} \cos \phi_{\text{eq}} [\epsilon_{n-1} + \epsilon_{n+1}] \quad (44)$$

or

$$2\epsilon_n/\tilde{h}^2 = \epsilon_{n-1} + \epsilon_{n+1} . \quad (45)$$

We expect an exponentially decaying solution for ϵ_n for $n \gg 1$. So set

$$\epsilon_n \sim e^{-na/\xi} \quad (46)$$

so that

$$2/\tilde{h}^2 = e^{a/\xi} + e^{-a/\xi} , \quad (47)$$

from which we get

$$e^{a/\xi} = \frac{1}{\tilde{h}^2} + \sqrt{\frac{1 - \tilde{h}^4}{\tilde{h}^4}} . \quad (48)$$

For small \tilde{h} , we get $\xi \approx a/(2|\ln \tilde{h}|)$. For $\tilde{h} \rightarrow 1$, we get $\xi = (a/2)(1 - \tilde{h})^{-1/2}$, in agreement with the continuum result. These results hold irrespective of the position of the center of the wall.

We now analyze the solution near the wall for small \tilde{h} . To do that we first look at Eq. (43) for ϕ_1 when we set $\phi_j = \pi/2 - \epsilon_j$:

$$\tilde{h} \cot \epsilon_1 = \frac{1}{2}[\cos \epsilon_2 - \cos \epsilon_1] . \quad (49)$$

But $\epsilon_2 \ll \epsilon_1$, so

$$\frac{\tilde{h}}{\epsilon_1} = \frac{1}{2} \left[1 - \left(1 - \frac{1}{2} \epsilon_1^2 \right) \right] = \frac{1}{4} \epsilon_1^2 . \quad (50)$$

So

$$\epsilon_1 = (4\tilde{h})^{1/3} . \quad (51)$$

From here on one should interpret \tilde{h} to mean $|\tilde{h}|$. Next, look at the equation for $\phi_2 = \pi/2 - \epsilon_2$:

$$\tilde{h} \cot \epsilon_2 = \frac{1}{2} [\cos \epsilon_1 + \cos \epsilon_3] \approx 1 . \quad (52)$$

In this way we find that $\epsilon_n = \tilde{h}$, for $n > 1$.

A more systematic approach shows that we can write the solution for the ϵ 's as

$$\epsilon_1 = (4\tilde{h})^{1/3} F_1[(4\tilde{h})^{2/3}] , \quad \epsilon_n = \epsilon_{\text{eq}} + A_n (4\tilde{h})^{2n-(7/3)} F_n[(4\tilde{h})^{2/3}] , \quad n > 1 , \quad (53)$$

where $A_n = 2^{(6-5n)}$, $\epsilon_{\text{eq}} = \sin^{-1} \tilde{h}$, and the functions F_n are analytic functions such that $F_n(0) = 1$.

To calculate E'' , note that, up to order $\tilde{h}^{4/3}$ in the energy, we may write

$$\begin{aligned} \sin \phi_1 &= \cos \epsilon_1 = 1 - \frac{1}{2} (4\tilde{h})^{2/3} [F_1(\tilde{h}^{2/3})]^2 + \frac{1}{24} (4\tilde{h})^{4/3} [F_1(\tilde{h}^{2/3})]^4 \dots \\ \sin \phi_j &= \cos \epsilon_j = 1 , \quad j > 1 ; \\ \cos \phi_1 &= \sin \epsilon_1 = (4\tilde{h})^{1/3} F_1(\tilde{h}^{2/3}) + O(\tilde{h}) \\ \cos \phi_j &= \sin \epsilon_j = O(\tilde{h}) , \quad j > 1 . \end{aligned} \quad (54)$$

Putting these evaluations into Eq. (41), we obtain

$$\begin{aligned} -E''/J &= 1 - \frac{1}{2} (4\tilde{h})^{2/3} [F_1(\tilde{h}^{2/3})]^2 + \frac{1}{24} (4\tilde{h})^{4/3} [F_1(\tilde{h}^{2/3})]^4 + (N-2) \\ &\quad - \frac{1}{2} \left[1 - (4\tilde{h})^{2/3} [F_1(\tilde{h}^{2/3})]^2 + \frac{1}{3} (4\tilde{h})^{4/3} [F_1(\tilde{h}^{2/3})]^4 \right] + \frac{1}{2} + 2\tilde{h} [(4\tilde{h})^{1/3} F_1(\tilde{h}^{2/3})] \\ &= N - 1 + (3/8) (4\tilde{h})^{4/3} + O(\tilde{h}^2) . \end{aligned} \quad (55)$$

where we used the definition that $F_1(0) = 1$. Then the wall energy is

$$E_w''/J = -(N-1) - (3/8) (4\tilde{h})^{4/3} + N = 1 - (3/8) (4\tilde{h})^{4/3} . \quad (56)$$

Note that this result is *not* identical to the case when the center of the wall is at a lattice site. The physics of this result will be discussed in more detail in the next section.

D. Quantum Domain Wall for Large S

We now consider the quantum chain for large S . For a chain of L spins of magnitude S , there are $2LS + 1$ states which have the same $h = 0$ ground state energy and which therefore must be treated within degenerate perturbation theory. Numerical studies show that for $S > 1$, this manifold of states splits into bands which are slightly different depending on whether $2S$ is even or odd. For S half integer there are $2S$ bands, each having L states except for the middle band which has $L + 1$ states. Approximately, the centers of these bands are at energies

$$\frac{1}{2}(L - 1)J + \frac{1}{2S}mH, \quad (57)$$

where m assumes the values $0, \pm 3/2, \pm 5/2, \dots \pm S$. For integer S one has $2S - 1$ bands, each having L states except for the middle band which has $2L + 1$ states. In this case the centers of the bands are given by Eq. (57), but m assumes the values $0, \pm 2, \pm 3, \dots, \pm S$. As an example, in Fig. 8 we show the density of states for $S = 3$ within the manifold \mathcal{M} . As Fig. 8 illustrates, the bands become wider and the gaps between bands become smaller as one approaches zero energy (about which the levels occur symmetrically). A qualitative explanation of the occurrence of such band gaps is as follows. If the spin $1/2$ case is likened to a hopping model, then the spin S case is analogous to a hopping model in which there is a periodically variable hopping matrix element. This problem is therefore analogous to that of an electron in a weak periodic potential, where one knows¹⁶ that even for arbitrarily weak potentials one has band gaps.

We will now demonstrate the existence of the band gaps and obtain quantitative information on the band widths for $h \ll 1$ as follows. We will give a construction for the outermost (and narrowest) sub-band, for which $m = S$ in Eq. (57). Consider the submanifold of states, \mathcal{M}_S , which contains the states, shown in Fig. 5, $|p\rangle$ (for $p = 1, 2, \dots, L$). These states are defined so that all spins (if any) having $i < p$ have $S_{iz} = S$, all spins (if any) having $i > p$ have $S_{iz} = -S$, and $S_{px} = S$. One may verify that the state $|n\rangle$ is in the

subspace \mathcal{M} of states of minimum energy eigenstates, E_0 , of the $h = 0$ Hamiltonian, i.e., that $J/(2S^2) \sum_{i=0}^{L+1} S_{iz} S_{i+1,z} |n\rangle = E_0 |n\rangle$. The states $|n\rangle$ are not orthogonal to one another, but do have an overlap which is small for large S and is given by

$$\langle p|p+1\rangle = \langle S_z = S|S_x = S\rangle^2 \equiv \tau, \quad (58)$$

for $0 < p < L$. Rose¹⁷ shows that

$$\langle S_z = S|S_x = S\rangle = D_{S,S}^{(S)}(0, \pi/2, 0) = 2^{-S}, \quad (59)$$

where \mathbf{D} is a rotation matrix. Therefore, we use states which are orthonormalized to leading order in τ ,

$$|\tilde{n}\rangle = |n\rangle - (\tau/2)|n+1\rangle - (\tau/2)|n-1\rangle, \quad (60)$$

where we interpret $|0\rangle$ and $|L+1\rangle$ to be zero.

We now work only to first order in τ . Then one notes that unless $n-1 \leq k \leq n+1$, $hS_{kx}|n\rangle$ has zero overlap with the subspace \mathcal{M} . To see this, note that $\langle S_z = m|S_x|S_z = m\rangle = 0$. Therefore we write, correct to leading order in τ ,

$$\begin{aligned} \langle \tilde{n} | \tilde{\mathcal{H}} | \tilde{n} + 1 \rangle &= \langle n | \tilde{\mathcal{H}} | n + 1 \rangle - (\tau/2) \langle n | \tilde{\mathcal{H}} | n \rangle - (\tau/2) \langle n + 1 | \tilde{\mathcal{H}} | n + 1 \rangle \\ &= -\frac{H}{2S} \sum_{k=n-1}^{n+1} \left(\langle n | S_{kx} | n + 1 \rangle - (\tau/2) \langle n | S_{kx} | n \rangle - (\tau/2) \langle n + 1 | S_{kx} | n + 1 \rangle \right) \\ &= -\frac{H}{2S} \left(\langle n | S_{nx} + S_{n+1,x} | n + 1 \rangle - (\tau/2) \langle n | S_{nx} | n \rangle - (\tau/2) \langle n + 1 | S_{n+1,x} | n + 1 \rangle \right) \\ &= -\frac{H}{2S} \left(2S \langle n | n + 1 \rangle - (S\tau/2) \langle n | n \rangle - (S\tau/2) \langle n + 1 | n + 1 \rangle \right) \\ &= -\frac{1}{2} H \tau = -H 2^{-2S-1}, \end{aligned} \quad (61)$$

where $\tilde{\mathcal{H}} \equiv \mathcal{H} - E_0$. Also

$$\langle \tilde{n} | \tilde{\mathcal{H}} | \tilde{n} \rangle = \langle n | \tilde{\mathcal{H}} | n \rangle + \mathcal{O}(\tau^2) = -\frac{H}{2S} \langle n | S_{nx} | n \rangle = -\frac{H}{2}. \quad (62)$$

Thus we expect this subspace of states with $S_x = S$ to form a sub-band centered at energy $E_0 - H/2$ with a width determined by the hopping matrix element¹⁸ $t(S) = -H 2^{-2S-1}$.

Thus the width of this band should be $4|t| = H2^{1-2S}$. Numerically, for $S = 5$ we found a band width of $0.002H$ in excellent agreement with our calculation. We thus have an analytic description of the outermost two sub-bands corresponding to $S_x = \pm S$. We did not consider an analysis of the remaining inner sub-bands. Note that the results shown in Fig. 8 are not for asymptotically large S . We did check that when S is large enough, the outermost subband does become symmetric, as one would expect for a one-dimensional density of states corresponding to Eqs. (61) and (62).

In a sense, one sees from this calculation that for the wall to move one lattice spacing, it must tunnel through the phase space of spin states indicated by the result of Eq. (59). In this connection a nice analogy has been suggested by Stinchcombe.¹⁹ Consider a rotor in a strong $\cos(2\theta)$ potential. One knows from exact solutions of the associated eigenvalue problem that one has a limit in which one has harmonic oscillator levels in the bottom of the potential well, all of which are doublets with a small tunnel splitting.²⁰ It is tempting to think that one can provide a field theory in one space and time dimension in which the single potential minimum of the rotor becomes a periodic potential in a lattice. Then the bands would reflect the tunnel splitting.

V. NATURE OF THE SPECTRUM

A. L^{-2} Spectrum in the Ferromagnetic Phase for Small S

So far, we have considered the form of the profiles $m(r)$ and have seen that at least qualitatively, their form can be understood from simple degenerate perturbation theory. The manifold \mathcal{M} considered consists of those states which give the lowest energies in the $h \rightarrow 0$ limit. For the case of $S = \frac{1}{2}$, for $h = 0$ these are the states shown in Fig. 5, namely,

$$|\uparrow\uparrow \cdots \uparrow\downarrow\rangle, \dots, |\uparrow \cdots \uparrow\downarrow \cdots \downarrow\rangle, \dots, |\uparrow\downarrow \cdots \downarrow\downarrow\rangle \quad (63)$$

and for L sites, there are $L + 1$ of them. For $S = 1$ one starts at $h = 0$ from the states

$$\begin{aligned}
& |\uparrow\uparrow \cdots \uparrow\downarrow\rangle, \dots, |\uparrow \cdots \uparrow\downarrow \cdots \downarrow\rangle, \dots, |\uparrow\downarrow \cdots \downarrow\downarrow\rangle \\
& |\uparrow\uparrow \cdots \uparrow 0 \downarrow\rangle, \dots, |\uparrow \cdots \uparrow 0 \downarrow \cdots \downarrow\rangle, \dots, |\uparrow 0 \downarrow \cdots \downarrow\downarrow\rangle
\end{aligned} \tag{64}$$

and one gets a subspace of $(L + 1) + L = 2L + 1$ states. All these states have in common that they contain a single wall. States which do not belong to this “one-particle subspace” \mathcal{M} have a large gap with the ground state. It is now remarkable that this clear separation of the subspace \mathcal{M} from all other states remains intact even for *finite* values of h . The subspace \mathcal{M} has a simple analogy for (anti)periodic boundary conditions. In these cases, \mathcal{H} commutes with the (modified) translation operator \mathcal{T} (or $\tilde{\mathcal{T}}$) and is thus decomposed into block diagonal form, the blocks being labeled by the eigenvalues of \mathcal{T} (or $\tilde{\mathcal{T}}$). \mathcal{M} corresponds to the set of lowest eigenstates of the blocks of \mathcal{H} .

While the gap of the lowest excited state *outside* \mathcal{M} with the ground state is finite (e.g. $1 - h$ for $S = \frac{1}{2}$ and when $\epsilon = 0$), the gaps inside \mathcal{M} scale with L^{-2} . If $g(i) = E_i - E_0$ denotes the i^{th} gap, we expect the scaling $g(i) \sim L^{-\theta}$ with $\theta = 2$, as obtained in Eq. (9). Finite-size estimates for θ are then obtained from, with $N = L + 2$

$$\theta_L = \frac{\ln(g(i)_{N+1}/g(i)_N)}{\ln(N/(N+1))} \tag{65}$$

The extrapolation towards the limit $N \rightarrow \infty$ was carried out with the BST extrapolation algorithm¹⁴. We illustrate the convergence of the finite-size data with a few examples for $S = 1$ in table I. The convergence towards $\theta = 2$ is even clearer for $S = \frac{1}{2}$.

We now consider the finite-size amplitudes

$$a(i) = N^2 g(i) . \tag{66}$$

The motivation for this comes from systems being precisely at a critical point. In that case, it is known that for one-dimensional quantum chains finite-size amplitudes defined as $Ng(i)$ are related¹⁵ to the anomalous dimensions of the scaling operators of the model and this leads to simple patterns of the spectrum of the amplitudes (see e.g. Ref. 14 for more information). Although we are not working here at a critical point, we observe a simple structure of the excited states within \mathcal{M} for $L \rightarrow \infty$ out of the critical region. Namely

$$r(i-1) = a(i-1)/a(1) = \frac{1}{3}(i-1)(i+1) \quad (67)$$

Evidence for this is presented in table II for $S = \frac{1}{2}$ and table III for $S = 1$ which give the BST extrapolated¹⁴ estimates for the $a(i)$. It is remarkable that the *same* expression should hold for the gaps ratios of both the $S = \frac{1}{2}$ and the $S = 1$ models, even though h is not very small and/or $\epsilon \neq 0$. For h small and $\epsilon = 0$, this result can be recovered from the energies (9) in lowest order of perturbation theory.

B. $L^{-\theta}$ Spectrum in the Oscillatory Phase for Small S

Turning to the oscillatory phase, we note that the spectrum of the states within the subspace \mathcal{M} is different from that in the F phase. Here there are important differences between L even and L odd.

For simplicity, we restrict attention to spin $S = \frac{1}{2}$ and first concentrate on the line $h = 0$. The structure of the levels we are going to find is shown in Fig. 9. For L even, the spectrum of the low-lying states corresponding to \mathcal{M} is grouped into doublets. While the doublet splitting is of order $\mathcal{O}(L^{-3})$, the gaps between doublets are of order $\mathcal{O}(L^{-2})$. For L odd, on the other hand, the energy levels are doubly degenerate, with gaps between them of order $\mathcal{O}(L^{-2})$.

To see this, we look for a scaling behavior of the energy gaps $g(i) = E_i - E_0 \sim L^{-\theta}$ and define finite-size estimates for the exponent θ using (65). In table V, we give our results for $\epsilon = 0.02$. For L even, estimates of θ from the lowest six gaps ($i = 1, \dots, 6$) are given. (For some of the higher gaps, the finite-size data for L small are not yet in the asymptotic regime and are thus discarded.) We observe that the lowest gap scales with an exponent $\theta = 3$, while all the higher gaps scale with $\theta = 2$. For L odd, on the other hand, each energy level is doubly degenerate even for finite L , i.e. $g(2j) = g(2j-1)$, $j = 1, 2, \dots$. Estimates of θ for $i = 2, 4, 6$ are given in table V and we find $\theta = 2$ throughout. Similar results are also found for $\epsilon = 0.1$ and 0.5 .

Next, we study the finite-size amplitudes $a(i) = N^2(E_i - E_0)$, with $N = L + 2$. Estimates for the lowest six amplitudes extrapolated to $L \rightarrow \infty$ are shown in table VI, obtained for L even or odd, respectively. We find that for L even, the estimates for pairs of amplitudes are quite close to each other and are consistent with being equal. Furthermore, their numerical values are near to the ones found for L odd. Taken together, the present data suggest the simple picture that in the $L \rightarrow \infty$ limit, the amplitudes $a(i)$ should become doubly degenerate and independent of the evenness or oddness of L . Finally, when looking for the amplitude ratios $a(i)/a(2)$, we find the following pattern

$$0, 1, 1, \frac{8}{3}, \frac{8}{3}, 5, \dots \quad (68)$$

which is consistent with the very same structure (67) of the low-lying amplitudes found on the $\epsilon = 0$ line. This finding is certainly consistent with the relationship between the order parameter profiles observed earlier (see Fig. 7) between systems on the $h = 0$ and $\epsilon = 0$ lines.

These findings can be reproduced from the perturbative arguments of section III.B when ϵ is small. For L odd, the eigenvalue problem then reduces to one treated there, but with $(L + 1)/2$ sites and $h \rightarrow -\epsilon$ and each state being twofold degenerate. For L even, we get two distinct problems, one with $L/2$ sites and one with $L/2 + 1$ sites. Using the expression (9) for the energies, we find pairs of levels with a splitting of order $\mathcal{O}(L^{-3})$ between them.

Qualitatively, the same structure persists throughout the O phase. We illustrate this in Fig. 10, where we show for $\epsilon = 0.25$ and $L = 10$ sites the dependence of the first few eigenvalues on h . Because L is not very large, the statements we shall make about the spectrum apply most strongly to the lowest levels and less well to the higher levels. We see that inside the O phase, the lowest energies occur in pairs which oscillate around another. In the ground state, there are for L sites $(L + 1)/2$ level crossings for L odd and $L/2$ level crossings for L even, respectively. These level crossing do not continue into the F phase. Finally, we point out that at the F/D transition, the energies combine into a $\left(\frac{1}{2}\right)$ representation of the $c = \frac{1}{2}$ Virasoro algebra, as predicted from conformal invariance^{14,21}. In

agreement with that prediction, we observe in Fig. 10 close to the critical point $h_c = 1 + \epsilon$ an (approximately) equidistant level spacing with the degeneracies $1, 1, 1, 1, 2, \dots$ (Actually, because of finite size effects, this structure is realized at $h = 1.15$ rather than at $h = h_c = 1.25$.)

This kind of level crossings in the ground state of finite-lattice quantum system has been first investigated for *periodic* boundary conditions²². There it was noted that the level crossings always occurred between the Z_2 even and odd sectors of the model. Here we find that the level crossing persist even if the Z_2 symmetry is broken by our chosen “up-down” boundary conditions (5). Applying finite-size scaling²² to the location h_k of the level crossings, we expect (but did not test) a scaling $h_k(L) - h^* \sim L^{-1/\nu}$. For periodic boundary conditions it is known²² that $\nu = 1/2$. ($h^* = \sqrt{4\epsilon}$ gives the O/F transition line).

C. Intrinsic Wall Width

It is obvious that the fact that the width of the wall for the quantum model is of order the system size is a result of a quantum superposition of states each of which have a narrow wall. It is tempting, therefore, to introduce a measure of the “intrinsic” width of the wall, which is the minimum width obtainable within the subspace of states under consideration. We emphasize that this concept depends on the subspace of states being considered. As we vary ϵ , the strength of the y - y coupling, it seems plausible that the character of the low lying “particle” states may vary. Thus, it would be of interest to introduce a measure of the intrinsic width applicable to this case. For this purpose consider the quantity Q defined as

$$Q = (2S)^{-1} \text{Max}_{n \in \mathcal{M}} \langle n | S_z(i) - S_z(i+1) | n \rangle , \quad (69)$$

where the maximum is to be taken over all possible quantum states $|n\rangle$ in the subspace \mathcal{M} . (As long as the site i is not near an end, Q will depend only weakly on i .) If the states consist of sharp walls, then Q will be unity. So we use this quantity to define the intrinsic width, W_i , via $W_i \sim 1/Q$. This type of definition is somewhat similar to the inverse participation

ratio introduced to characterize localized and extended states of an electron in a random potential.²³ Here we take the subspace \mathcal{M} to be the “particle” subspace of states. This definition is appropriate as long as the subspace of particle states can be unambiguously separated from the continuum. This requirement suggests that $h \ll J$. But, we can also use this idea when ϵ is nonzero.

We should mention that the maximization required in Eq. (69) is easy to carry out. One simply forms the matrix, \mathbf{P} , (in any representation) where

$$\mathbf{P}_{n,m} = (2S)^{-1} \langle n | S_z(i) - S_z(i+1) | m \rangle , \quad (70)$$

and Q is the largest eigenvalue of \mathbf{P} . When Q is less than unity, one also obtains information on the shape of the wall via the eigenvalue spectrum of \mathbf{P} . For instance, if the wall has width 3, and if the three largest eigenvalues of \mathbf{P} are degenerate, then one would conclude that the intrinsic wall profile is linear.

One context in which this concept provides some information is when we consider the large S limit of the transverse Ising model. In that case we have already seen that the low lying particle spectrum splits into bands corresponding roughly to values of S_x . When we apply Eq. (69) taking the subspace \mathcal{M} to be the lowest band of L states with $S_x = S$, we expect to find $Q = 1/2$. We in fact verified this expectation in our numerical calculations. They showed that one obtains two nearly degenerate maximal eigenvalues of magnitude essentially equal to $1/2$. There are two eigenvalues because there are two wavefunctions which can maximize Q since the minimum intrinsic wall width is two lattice spacings. We see then, that the prescription of Eq. (69) coincides with the perturbative calculations for small h .

D. Barrier to Domain Wall Motion

First we summarize the result for the classical ($S \rightarrow \infty$) system. Note that $E'_w < E''_w$, for small H . So to move the wall through one or more lattice constants requires an energy

$$\Delta = E''_w - E'_w = J \left[\tilde{h} - (3/8)(4\tilde{h})^{4/3} \right]. \quad (71)$$

We have numerically studied the energies of the classical domain wall when its center is either at a lattice site or midway between lattice sites. We find that the barrier energy Δ does not change sign as H is increased as might be suggested by Eq. (71), but rather Δ decreases monotonically to zero as H is increased towards its critical value of unity.

We carried out similar calculations for quantum systems with $S = \frac{1}{2}$ and $S = 1$. We found that the difference in energy when the center of the wall moved from a lattice site to a point midway between lattice sites was too small to be accessible to double precision arithmetic. Since, for a chain of length $L < 20$, we can not imagine a parameter on such a scale, we assert that the quantum barrier energy is zero. Practically, we performed this test as follows. For sufficiently large lattice sizes L , we expect for the ground state energies $E_0(2N)$ (i.e. wall between two sites) and $E_0(2N+1)$ (i.e. wall at a site)

$$\begin{cases} E_0(2N) = A \cdot 2N + B + \dots \\ E_0(2N+1) = A \cdot (2N+1) + B' + \dots \end{cases}, \quad (72)$$

where A is the ground state energy per spin and independent of the boundary conditions. For $S = \frac{1}{2}$, $A = -\frac{1}{\pi}(h+1)E(\sqrt{4h}/(h+1))$ where E is a complete elliptic integral²⁴. The desired wall energy difference should be proportional to $B - B'$. This in turn can be estimated from the quantities

$$\begin{aligned} p_N &= E_0(2N+1) + E_0(2N-1) - 2E_0(2N) \simeq 2(B' - B) + \dots \\ q_N &= E_0(2N+2) + E_0(2N) - 2E_0(2N+1) \simeq 2(B - B') + \dots \end{aligned} \quad (73)$$

and we note that p_N and q_N should have opposite signs. We give in table IV estimates for both p_N and q_N for both $S = \frac{1}{2}$ and $S = 1$ for $h = 0.1$. We chose this value of h to be small enough that is was for from criticality but large enough so that $|B - B'|$ should be easily observable if nonzero. Taking the entries at face value, the wall energies must be less than $\mathcal{O}(10^{-5})$. Moreover, since p and q should have opposite signs, the values given

in table IV appear to be entirely due to the leading finite-size corrections and we find that p_N, q_N decrease rapidly with increasing N . So we get an upper bound

$$\text{barrier energy} \sim |B - B'| \leq \mathcal{O}(10^{-8}) \quad (74)$$

for both $S = \frac{1}{2}$ and $S = 1$. This result is not surprising. In the limit when the width of the domain wall diverges (as it does for $L \rightarrow \infty$), the barrier energy should vanish. Whether it vanishes algebraically or exponentially would require further numerical or analytic analysis.

E. Crossover From Quantum to Classical Behavior

Here we discuss the various regimes which exist at large S . It is clear that bands of energy levels exist on various scales. It is useful to discuss the consequences of these energy scales in terms of scaling functions. For notational simplicity, in this subsection $F(x)$ will denote a scaling function of x which, in general, will be different in different appearances.

We first discuss the thermodynamic properties of the wall. For this purpose we will consider the entropy associated with the wall, S_w , defined as the entropy with “up-down” boundary conditions minus that with “up-up” boundary conditions. We emphasize that the scaling of the bulk thermodynamics, i.e., the extensive part of the thermodynamic potentials is independent of the boundary conditions and only depends on the bulk thermodynamic variables.²⁵ At temperatures small compared to J/S the entropy with “up-up” boundary conditions will be zero, because the ground state is nondegenerate. The entropy with “up-down” boundary conditions will be that due to the band of states with just one domain wall. First there is an extreme low-temperature limit in which the entropy is vanishingly small:

$$S_w \approx 0 ; \quad T \ll H 2^{1-2S} L^{-2} , \quad (75)$$

where we always set k_B , the Boltzmann constant equal to unity. In this limit only the lowest single state of the tunneling band found in Sec. IVB comes into play. At higher temperatures the tunneling band is activated, so that

$$S_w = \ln L + F\left(\frac{T}{H2^{1-2S}}\right) ; \quad H2^{1-2S}L^{-2} \ll T \ll H/S . \quad (76)$$

Here $\ln L + F(x)$ is the entropy of a one dimensional tight binding band of L sites. By noting the form of the density of states one can see that for small x , $F(x) \sim (1/2) \ln x + \text{Const}$ and as $x \rightarrow \infty$, $F(x) \rightarrow 0$. The upper limit of this regime is defined so that essentially only the lowest subband of Sec. IVB is activated. Next, there is a regime when the temperature is high enough that all states of these subbands are equally populated, but only one domain wall exists. In this discussion it is assumed that $H \ll J/S$, so that the band of particle states is well separated from the states with more than one wall. In this regime one has

$$S_w = \ln(2SL) + F\left(\frac{T}{H}\right) , \quad H/S \ll T \ll J/S . \quad (77)$$

In this case, $F(x) \rightarrow 0$ for $x \rightarrow \infty$ and $F(x) \sim \ln(T/2H) + 1$ for $x \rightarrow 0$. Finally, we have the classical regime when $T \gg J/S$. In that regime any effects due to the fact that $S_x(i)$ and $S_z(i)$ do not commute with one another becomes unimportant. In that regime then, the partition function for the quantum model of Eq. (2) is the same [up to corrections of relative order $J/(ST)$] as that of the classical model in which the operators are interpreted as classical variables according to Eq. (16).

The effect of a random potential is somewhat different. In the present context a random potential would be created by a field which independently for each site assumes random values from a distribution of width V_R . It is known²⁶ that in the presence of a random potential all states are localized. That means that in the presence of a random field the eigenfunctions are localized and therefore the width of the wall in the ground state remains finite in the limit $L \rightarrow \infty$. Nevertheless, the width of the wall, W , can be expressed in terms of scaling functions of the same variables as describe the thermodynamics except that here V_R replaces T . Thus

$$W \sim L ; \quad V_R \ll H2^{1-2S}L^{-2} , \quad (78)$$

and

$$W/a = F\left(\frac{V_R}{H2^{1-2S}}\right) ; \quad H2^{1-2S}L^{-2} \ll V_R \ll H/S . \quad (79)$$

Since we know that W can not be less than the intrinsic width, we see that $F(\infty) = 2$.

Similarly, we have

$$W/a = F\left(\frac{V_R}{H}\right) ; \quad H/S \ll V_R \ll J/S . \quad (80)$$

In this case $F(0) = 2$ and $F(\infty) = 1$, the intrinsic wall width in this regime. For any larger V_R , W/a remains equal to unity.

VI. SUMMARY

We may summarize our conclusions for the Ising model in a transverse field as follows.

1. Although an exact analysis of domain walls in the transverse Ising model can in principle be accomplished using the Jordan-Wigner transformation, it is much simpler to consider the nature of degenerate perturbation theory in the presence of “up-down” boundary conditions. Within degenerate perturbation theory for $S = 1/2$ and $S = 1$ the Hamiltonian governing the position of the center of the domain wall is isomorphic with a hopping model with a hopping matrix element $t \sim H$. We verified this in detail with analysis of the scaling of the energy levels with chain length, L .
2. For spins $\frac{1}{2}$, 1 and $\frac{3}{2}$ the ground state profiles when spins at opposite ends of a chain of length L are fixed to be antiparallel show relatively little dependence on the transverse field h (as long as h is less than the critical value, h_c , above which ordering in S_z is destroyed). For small h the profiles at large but finite S are not very different from those at small S . In all cases, the profiles are quite well obtained from the hopping model.
3. The profiles in the oscillatory phase show much larger finite size corrections than those in the ferromagnetic phase. In the limit $L \rightarrow \infty$ the profiles in the oscillatory phase may still show some oscillatory behavior, unlike in the ferromagnetic

phase. Also, our results for the profiles show an interesting finite-size effect in which spatial parity appears to be broken.

4. In the spectrum of the oscillatory phase at $h = 0$ one finds an unusual pattern for the gaps between the ground state and the first few excited states. While for L even, the energies form doublets, each with a splitting which scales with L as L^{-3} , and with gaps between the doublets which scale as L^{-2} . For L odd, the energies are doubly degenerate and the gaps scale with L as L^{-2} . This behavior was explained in terms of dimer excitations which occur in the limit $h \rightarrow 0$ when $\epsilon \neq 0$.
5. For large S the quantum transverse Ising model the Hamiltonian describing the position of the center of the domain wall gives rise to band splittings analogous to those found for an electron in a periodic potential¹⁶. The lowest sub-band is described by a hopping model in which the center of the domain wall tunnels from one site to a neighboring sites. The associated tunneling matrix element is of order $hS \exp(-\alpha S)$, where $\alpha = 2 \ln 2$. It would be interesting to recover this result within a field theory for one space and one time dimension.
6. For the classical ($S = \infty$) model the domain wall is extremely narrow for small h . We have determined the domain wall energy for the case when i) the center of the domain wall is at a lattice site and ii) the center of the domain wall is midway between two lattice sites. The difference between these energies is the pinning energy which must be exceeded to move the domain wall through the lattice. For the quantum model we find this pinning energy vanishes as $L \rightarrow \infty$ due to the fact that the width of the domain wall diverges in this limit.
7. In attempting to relate quantum problems to classical problems it is necessary to define an intrinsic width, W_i , of a quantum domain wall. We have defined W_i as the minimum possible width attainable using wave functions from a manifold \mathcal{M} . At temperatures large compared to the band but small compared to the activation

energy for creation of an additional wall, the manifold \mathcal{M} is the hopping band. In that case, the intrinsic width of the quantum system is essentially equal to the width of the analogous classical domain wall.

Acknowledgements The authors appreciate helpful advice from D.B. Abraham, R. B. Stinchcombe, T. C. Lubensky, I. Affleck and J.L. Cardy. ABH thanks the Department of Theoretical Physics of Oxford University for its kind hospitality. ABH is supported by an EPSRC Visiting Fellowship and MH is supported by a grant from the EC programme “Human Capital and Mobility”. MC acknowledges support by the Polish Agency KBN (grant number 2 P302 127 07).

REFERENCES

- ¹ F. Family and T. Vicsek, editors, "Dynamics of Fractal Surfaces", World Scientific, Singapore (1991); G. Forgacs, R. Lipowsky and Th. M. Nieuwenhuizen, in "Phase Transitions and Critical Phenomena", edited by C. Domb and J. L. Lebowitz, Vol. 14, Academic Press, NY (1991).
- ² D. A. Huse and C. L. Henley, Phys. Rev. Lett. **54**, 2708 (1985).
- ³ A. J. Bray and M. A. Moore, Phys. Rev. Lett. **58**, 57 (1987); D. S. Fisher and D. A. Huse, *ibid* **56**, 1601 (1986).
- ⁴ M. Cieplak and J. R. Banavar, J. Phys. A **23**, 4385 (1990)
- ⁵ M. Cieplak and M. S. Li, Fractals **2**, 481 (1994).
- ⁶ M. Cieplak, A. Maritan, and J. R. Banavar, Phys. Rev. Lett. **72**, 2322 (1994)
- ⁷ M. Cieplak, and M. Robbins, Phys. Rev. Lett. **60**, 2042 (1988); N. Martys, M. Cieplak, and M. Robbins, *ibid* **66**, 1058 (1991).
- ⁸ M. O. Robbins and J. F. Joanny, Europhys. Lett. **3**, 729 (1987).
- ⁹ R. Lipowsky, Nature **349**, 475 (1991).
- ¹⁰ J. A. Thornton, Ann. Rev. Matter. Sci. **7**, 239 (1977).
- ¹¹ S. Katsura, Phys. Rev. **127**, 1508 (1962); T. Niemeyer, Physica **36**, 377 (1967); E. Barouch and B.M. McCoy, Phys. Rev. **A3**, 786 (1971)
- ¹² F. R. N. Nabarro, *Theory of Crystal Dislocations*, (Oxford University Press, Oxford, 1967), p175.
- ¹³ K. Uzelac and R. Jullien, J. Phys. **A14**, L151 (1981); C.J. Hamer, J. Phys. **A15**, L675 (1982).

- ¹⁴ P. Christe and M. Henkel, *Introduction to Conformal Invariance and Its Applications to Critical Phenomena*, (Springer, Berlin, Heidelberg, New York, 1993) Chap. 9.
- ¹⁵ J. L. Cardy, J. Phys. **A17**, L385 (1984).
- ¹⁶ N. W. Ashcroft and N. D. Mermin, *Solid State Physics* (Saunders College Publishing, New York, 1976).
- ¹⁷ M. E. Rose *Elementary Theory of Angular Momentum* (John Wiley, New York, 1957), p52.
- ¹⁸ This argument is correct to leading order in τ . It neglects overlap between $\mathcal{H}|n\rangle$ and other states of \mathcal{M} , notably states similar to $|n\rangle$, but in which S_{nx} has the value $S - 1$. However the band of the $S_x = S - 1$ states is separated from the band of $S_x = S$ states by an energy approximately equal to $H/(2S)$. But since the relevant matrix element is of order $\tau H \ll H$ and is off-diagonal, it will enter at order $(\tau H)^2/[H/(2S)] \sim S\tau^2$. Thus this effect is negligible compared to the terms we do treat, at least for large S .
- ¹⁹ R. B. Stinchcombe, private communication.
- ²⁰ T. E. Stern, Proc. Roy. Soc. A130, 551 (1931).
- ²¹ J.L. Cardy, Nucl. Phys. **B275**, 200 (1986); A.I. Bugrij and V.N. Shadura, Phys. Lett. **150A**, 171 (1990).
- ²² C. Hoeger, G.v. Gehlen and V. Rittenberg, J. Phys. **A18**, 1813 (1985).
- ²³ R. J. Bell and P. Dean, Disc. Faraday Soc. **50**, 55 (1970).
- ²⁴ P. Pfeuty, Ann. of Phys. **57**, 79 (1970)
- ²⁵ M. N. Barber in *Phase Transitions and Critical Phenomena*, Vol. 8, Eds. C. Domb and J. Lebowitz, (Academic Press New York 1983), p. 145; V. Privman (Ed), *Finite Size Scaling and Numerical Simulation of Statistical Systems*, (World Scientific, Singapore 1990).

²⁶ For a review of localization questions see D. J. Thouless, Phys. Rep. **13**, 93 (1974).

TABLES

TABLE I. Finite-size estimates of the exponent θ for the spin-1 model for two values of h .

The line labeled ∞ gives the $L \rightarrow \infty$ estimates and the numbers in brackets give the estimated uncertainty in the last given digit.

ϵ	$h = 0.70711$			$h = 0.141421$		
5	2.1178266444	1.8259262012	1.6349745596	1.9232489201	1.5981924835	1.5459794089
6	2.1844497668	1.9905134772	1.7373695512	2.0506897828	1.8186085947	1.5210107108
7	2.2059303628	2.0578126044	1.9022922190	2.1146816632	1.9229956697	1.7423552051
8	2.2066110482	2.0951905179	1.9690586873	2.1430516979	1.9914094495	1.8343490446
9	2.1989322892	2.1141764054	2.0126854700	2.1534693122	2.0339467283	1.9014943987
10	2.1883357907	2.1226007841	2.0407754063	2.1549673204	2.0598773753	1.9493182117
11	2.1771411322	2.1251001574	2.0585469560	2.1520791521	2.0754047064	1.9830416672
12	2.1663136392	2.1243123257	2.0695528139	2.1471130353	2.0844025361	2.0068020462
13	2.1562240067	2.1217337201	2.0761282137	2.1412643703	2.0892668405	2.0235701176
∞	2.0000(1)	2.000(2)	2.01(2)	2.000(2)	2.00(2)	2.06(8)

TABLE II. Extrapolated estimates for the finite-size scaling amplitudes $a(i)$ for $S = \frac{1}{2}$ in the ferromagnetic phase F. The last column gives the amplitude ratios $r(i) = a(i)/a(1)$ from Eq. (67).

Gap Nr.	$h = 0.1$	$h = 0.1$	$h = 0.2$	$h = 0.2$	$h = 0.5$	$h = 1$	$r(i)$
	$\epsilon = 0$	$\epsilon = 0.0025$	$\epsilon = 0$	$\epsilon = 0.01$	$\epsilon = 0$	$\epsilon = 0.2$	
1	1.64492(2)	1.480441(3)	3.70110(1)	2.960882(1)	14.803(3)	29.272(3)	1
2	4.38641(2)	3.94784(1)	9.8695(4)	7.895688(2)	39.406(2)	79.998(40)	$\frac{8}{3}$
3	8.2247(1)	7.40221(2)	18.5054(3)	14.804388(3)	73.865(8)	146.31(10)	5
4	13.1595(8)	11.8435(1)	29.604(8)	23.68675(8)	118.2(2)	233.9(5)	8
5	19.190(2)	17.2719(2)	43.168(4)	34.542(1)	172.5(2)		$\frac{35}{3}$
6	26.312(5)	23.687(2)	59.13(2)	47.371(3)	236.5(3)		16

TABLE III. Extrapolated estimates for the finite-size amplitudes $a(i)$ for spin $S = 1$.

	h			
i	0.007071	0.035355	0.070711	0.141421
1	0.0377469	0.20378(8)	0.44676(3)	1.0697(10)
2	0.10066	0.5434(6)	1.19141(15)	2.866(10)
3	0.1888(2)	1.019(5)	2.234(5)	5.35(2)
4	0.302(1)	1.67(5)	3.58(8)	8.55(10)
5	0.444(4)			
6	0.605(8)			

TABLE IV. Estimates for $10^5 p_N$ and $10^5 q_N$, giving upper bounds for the wall energy differences $2|B - B'|$ at $h = 0.1$

	Spin $\frac{1}{2}$		Spin 1	
N	p_N	q_N	p_N	q_N
2	224.4	124.0	102.1	48.9
3	73.9	46.7	26.2	15.3
4	30.9	21.3	9.5	6.2
5	15.1	11.0	4.2	
6	8.2	6.3		
7	4.8	3.8		
8	3.0	2.5		

TABLE V. Finite-size data for the exponent θ obtained for $S = \frac{1}{2}$ with $h = 0$ and $\epsilon = 0.02$ and the extrapolated limit for $L \rightarrow \infty$. Estimates obtained for L even and odd, respectively, are shown separately.

L							L			
6	2.45042	1.19367	1.37847	0.80651			5	1.01958		
8	2.58995	1.38695	1.65858	1.13219	1.12909	0.74787	7	1.36641	0.92322	
10	2.67304	1.50917	1.78977	1.32647	1.44186	1.05893	9	1.54228	1.25898	0.83163
12	2.72829	1.59281	1.86194	1.45465	1.61033	1.25543	11	1.64710	1.44770	1.15571
14	2.76770	1.65329	1.90568	1.54487	1.71252	1.38993	13	1.71580	1.56697	1.35237
16	2.79721	1.69886	1.93399	1.61140	1.77947	1.48709	15	1.76383	1.64816	1.48286
							17	1.79902	1.70640	1.57477
∞	2.995(5)	2.00(2)	2.01(2)	1.98(3)	2.01(1)	1.99(3)	∞	1.999(2)	1.99(1)	2.00(1)

TABLE VI. Extrapolated finite-size amplitudes $a(i)$, $i = 1, 2, \dots, 6$ for $S = \frac{1}{2}$ with $h = 0$ and for several values of ϵ . For a given ϵ , the first (second) line corresponds to the estimates found for L even (odd).

ϵ	1	2	3	4	5	6
0.02	0	1.2033(20)	1.22(4)	3.191(20)	3.243(15)	5.97(10)
	0	1.203(3)	1.203(3)	3.191(15)	3.191(15)	5.975(20)
0.10	0	6.553(15)	6.58(3)	17.26(15)	17.59(10)	32.3(3)
	0	6.555(20)	6.555(20)	17.32(8)	17.32(8)	32.48(10)
0.50	0	57.2(9)	58.8(6)	153(4)	158(3)	311(9)
	0	58.3(3)	58.3(3)	156(2)	156(2)	325(10)

FIGURE CAPTIONS

Fig. 1 Phase diagram of the “yz” model of Eq. (3) for spin $S = \frac{1}{2}$. The disordered (D), ferromagnetic (F) and oscillatory (O) phases are indicated.

Fig. 2 Local magnetization profile $m(r)$ for the spin- $\frac{1}{2}$ model with $h = 0.1$ and $\epsilon = 0$ for system sizes $L = 2 \dots 16$.

Fig. 3 Comparison of the magnetization profiles $m(r)$ for the spin- $\frac{1}{2}$ (boxes), the spin-1 (full circles) and the spin- $\frac{3}{2}$ (open circles) models. The full curve gives the profile of Eq. (11) which is correct to first order in h . The data are for $\epsilon = 0$ and A) $h = 0.1$ and B) $h = 0.5$.

Fig. 4 Magnetization profile $m(r)$ for three values of the transverse field h and for $\epsilon = 0$ and $S = \frac{1}{2}$.

Fig. 5 States in the ground manifold \mathcal{M} . Top: the states $|n\rangle$ introduced for spin $1/2$. Bottom: the states $|n\rangle$ introduced for the case $S \gg 1$. In this case the n th spin has $S_x = S$.

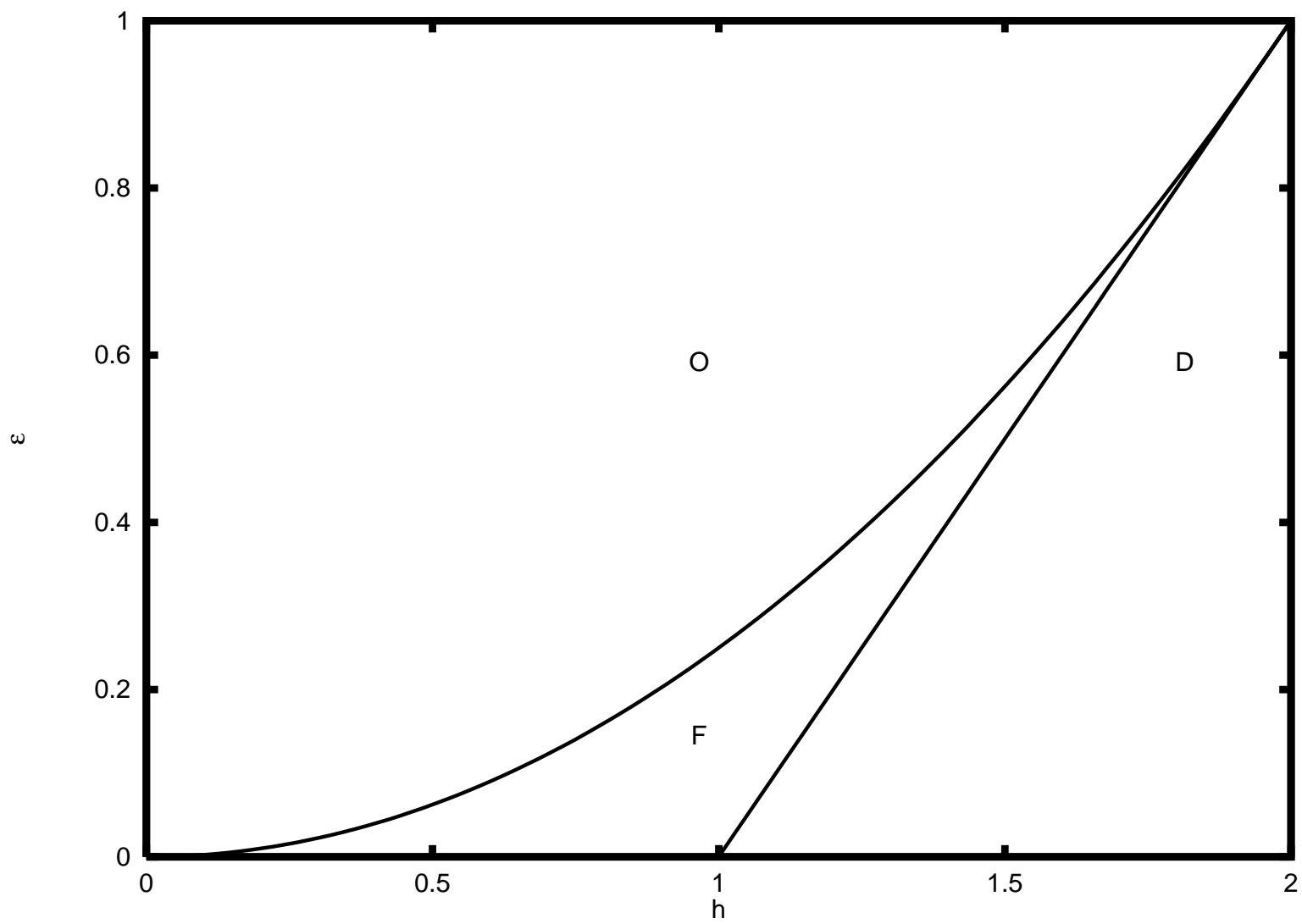
Fig. 6 Magnetization profile of the oscillatory phase of the spin- $\frac{1}{2}$ model with $\epsilon = 0.5$ and $h = 0.01$, for A) L even and B) L odd.

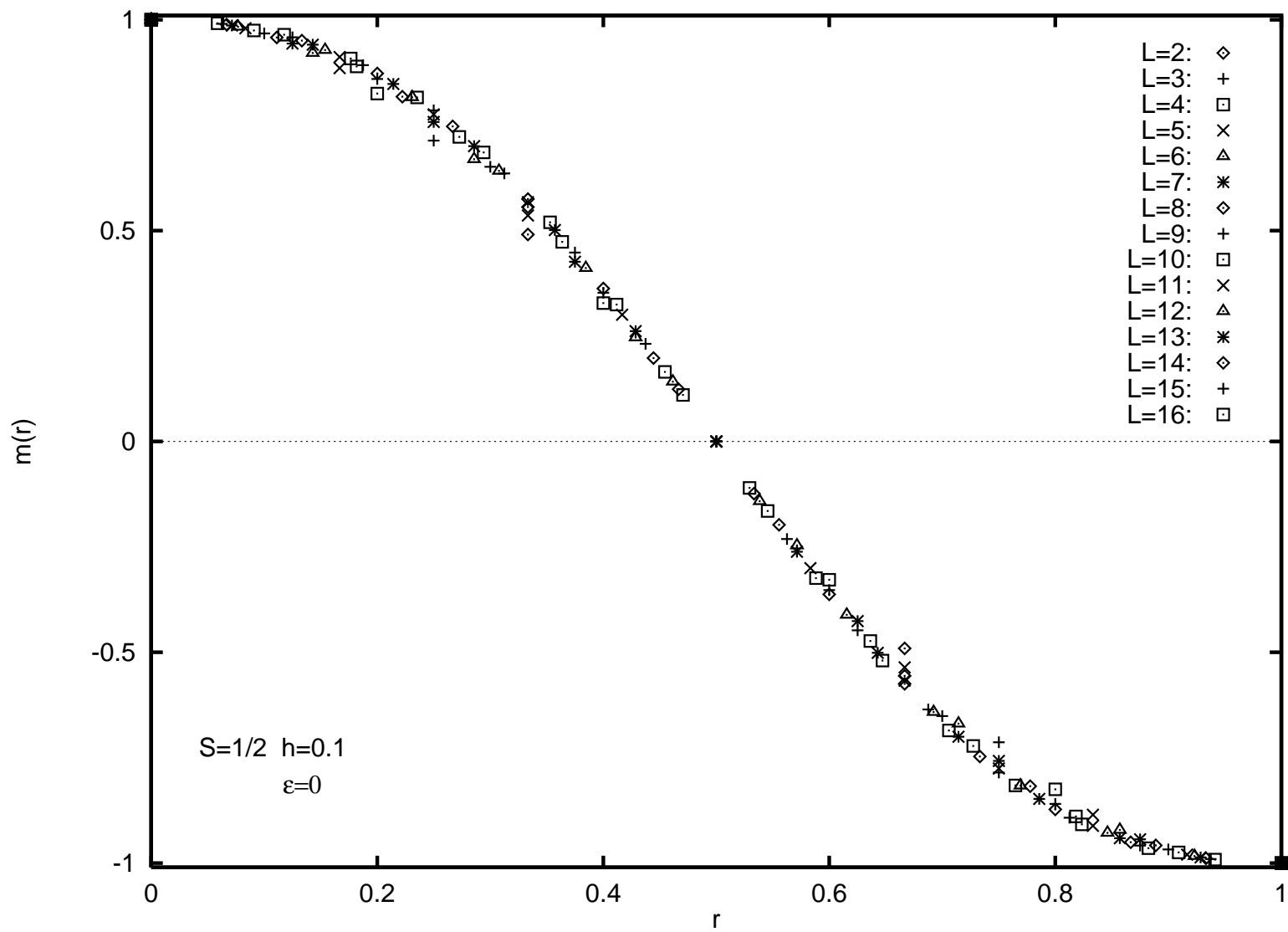
Fig. 7 Comparison of the magnetization profiles of the spin- $\frac{1}{2}$ model with $h \rightarrow 0$ and the values of ϵ indicated (data points) and with $h = h_{\text{eff}}(\epsilon) = \sqrt{\epsilon}$ and $\epsilon = 0$ (curves), for $L = 15$.

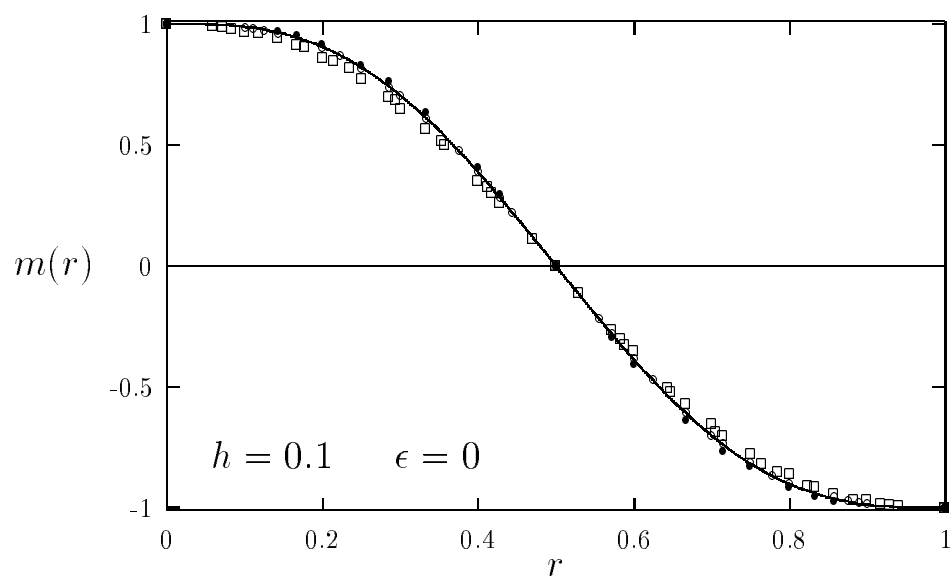
Fig. 8 Density of states (per site) $D(E)$ as a function of energy E (relative to the center of the manifold) within the manifold \mathcal{M} for $S = 3$. The middle subband contains $2L + 1$ states. The other subbands contain L states. The asymmetry of the subbands rapidly decreases as S increases. Inside each subband, near its edge at E_i , $D(E) \sim |E - E_i|^{-1/2}$ for $L \rightarrow \infty$.

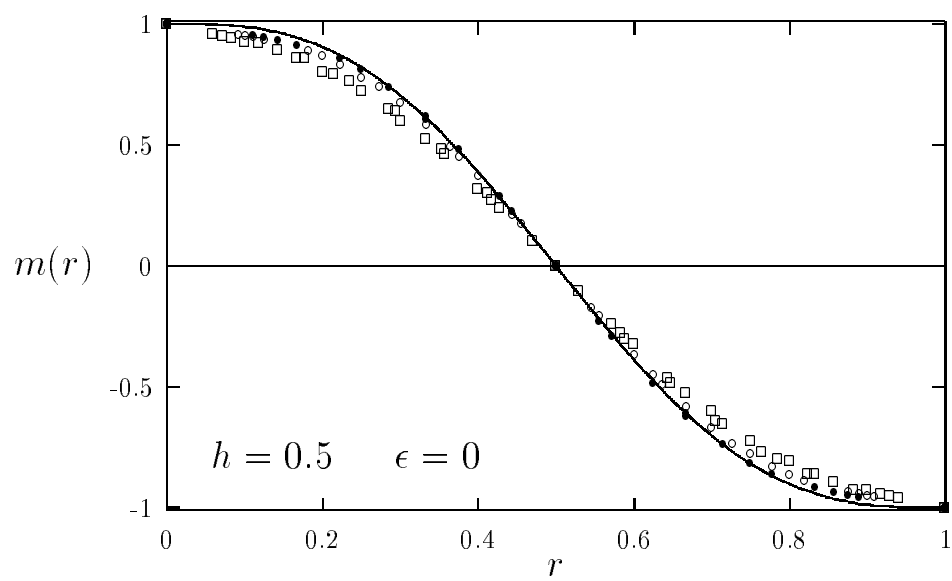
Fig. 9 Schematic structure of the low-lying states for spin $S = \frac{1}{2}$, $h = 0$ and $\epsilon \neq 0$, for A) L even and B) L odd.

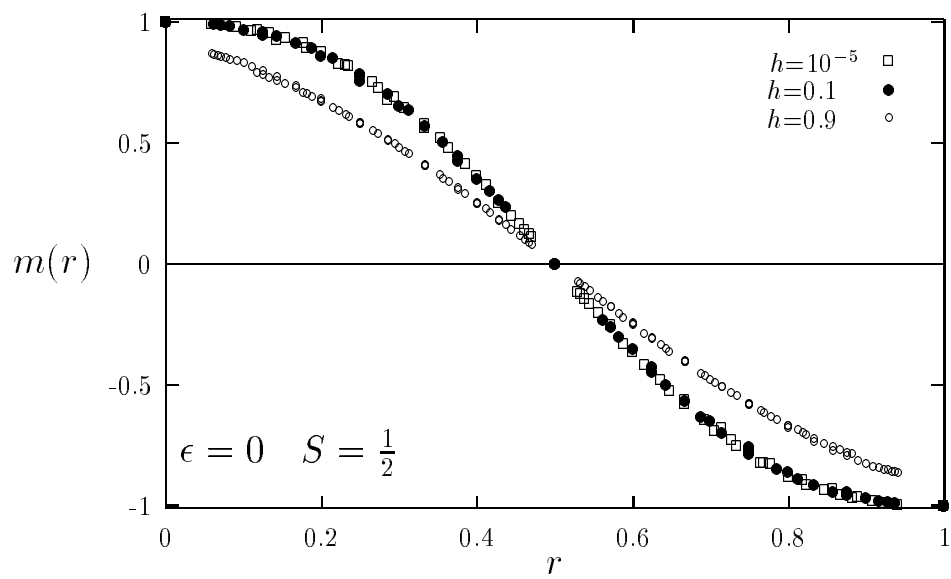
Fig. 10 Spectrum of \mathcal{H}_{yz} for spin $S = \frac{1}{2}$ and $\epsilon = 0.25$ as a function of h for $L = 10$ sites. The two vertical lines indicate the location of the transitions between the O/F phases and the F/D phases, respectively, for $L \rightarrow \infty$.

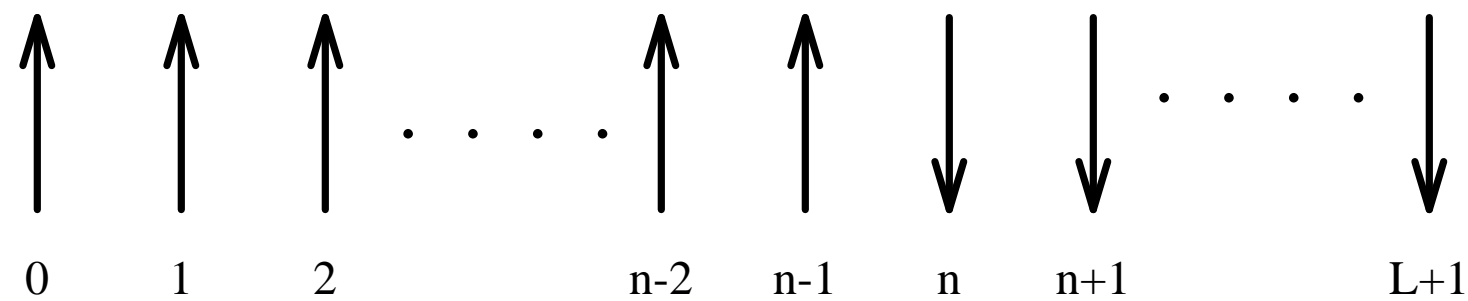




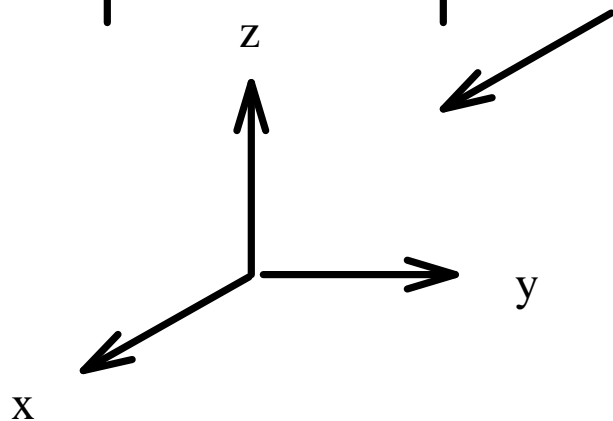
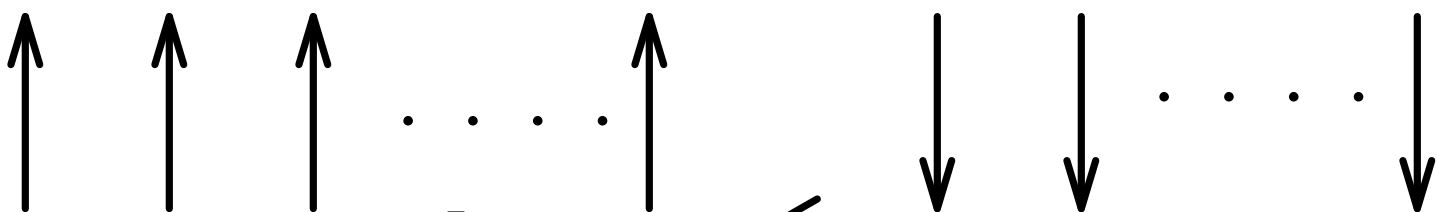


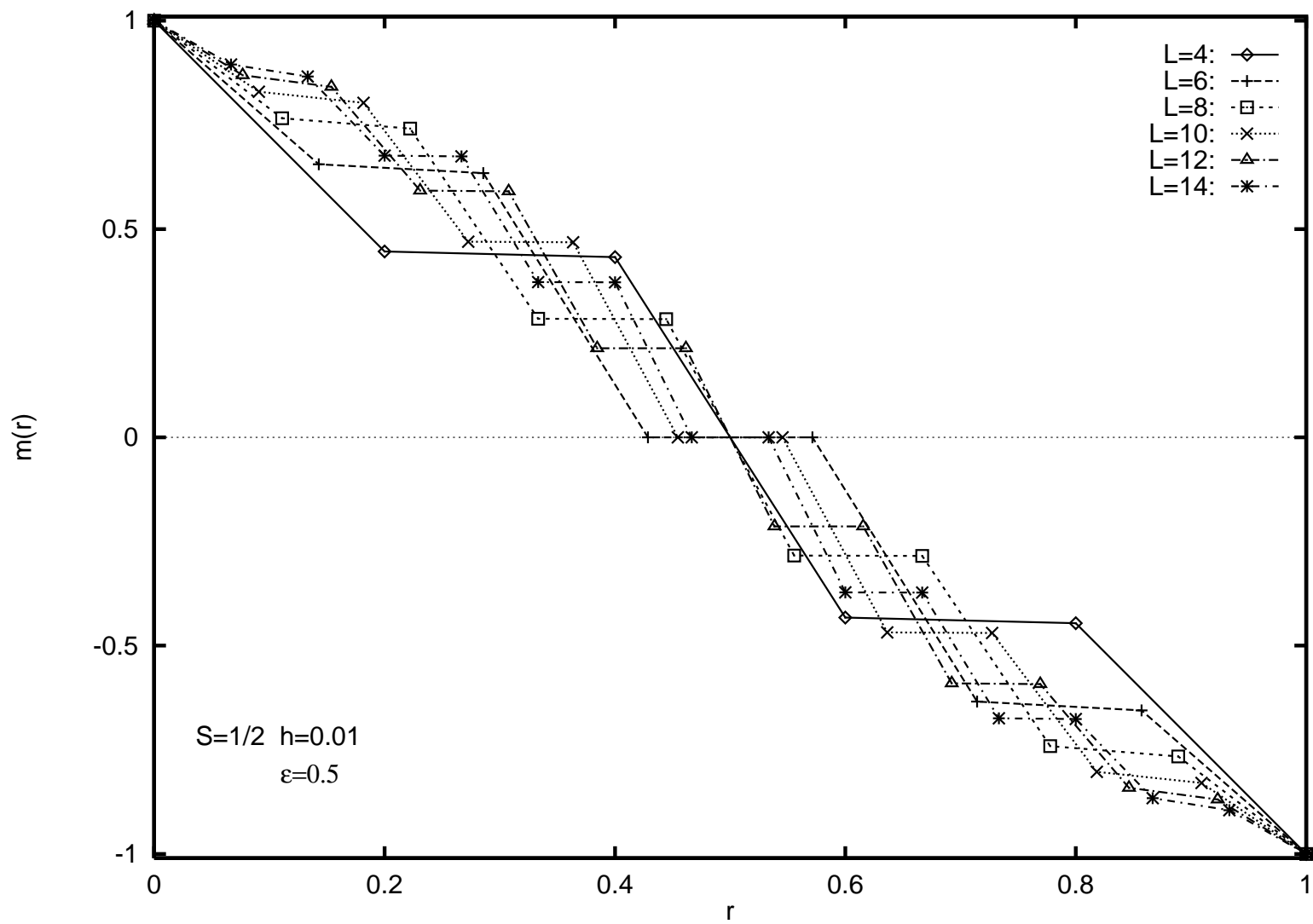


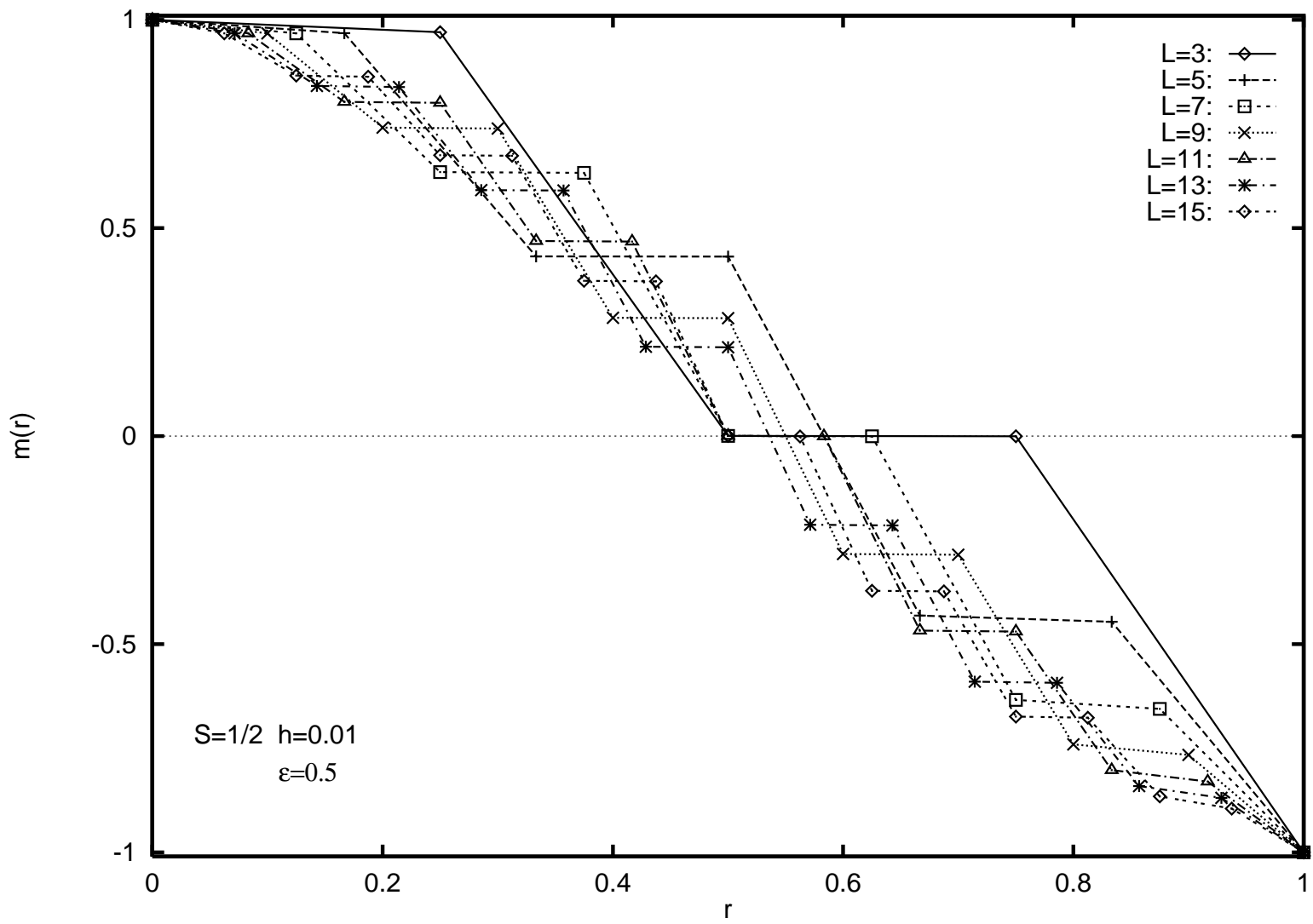


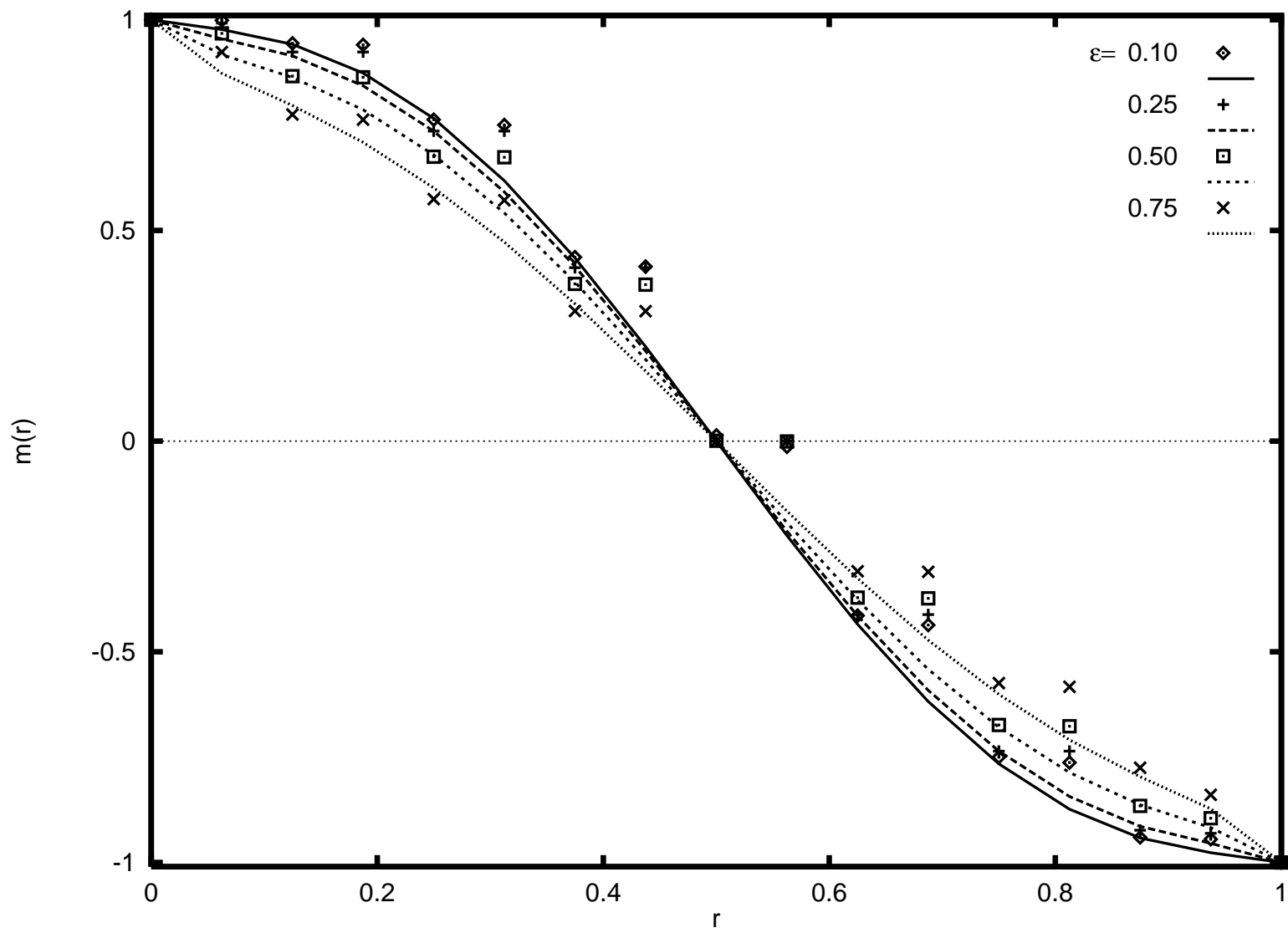


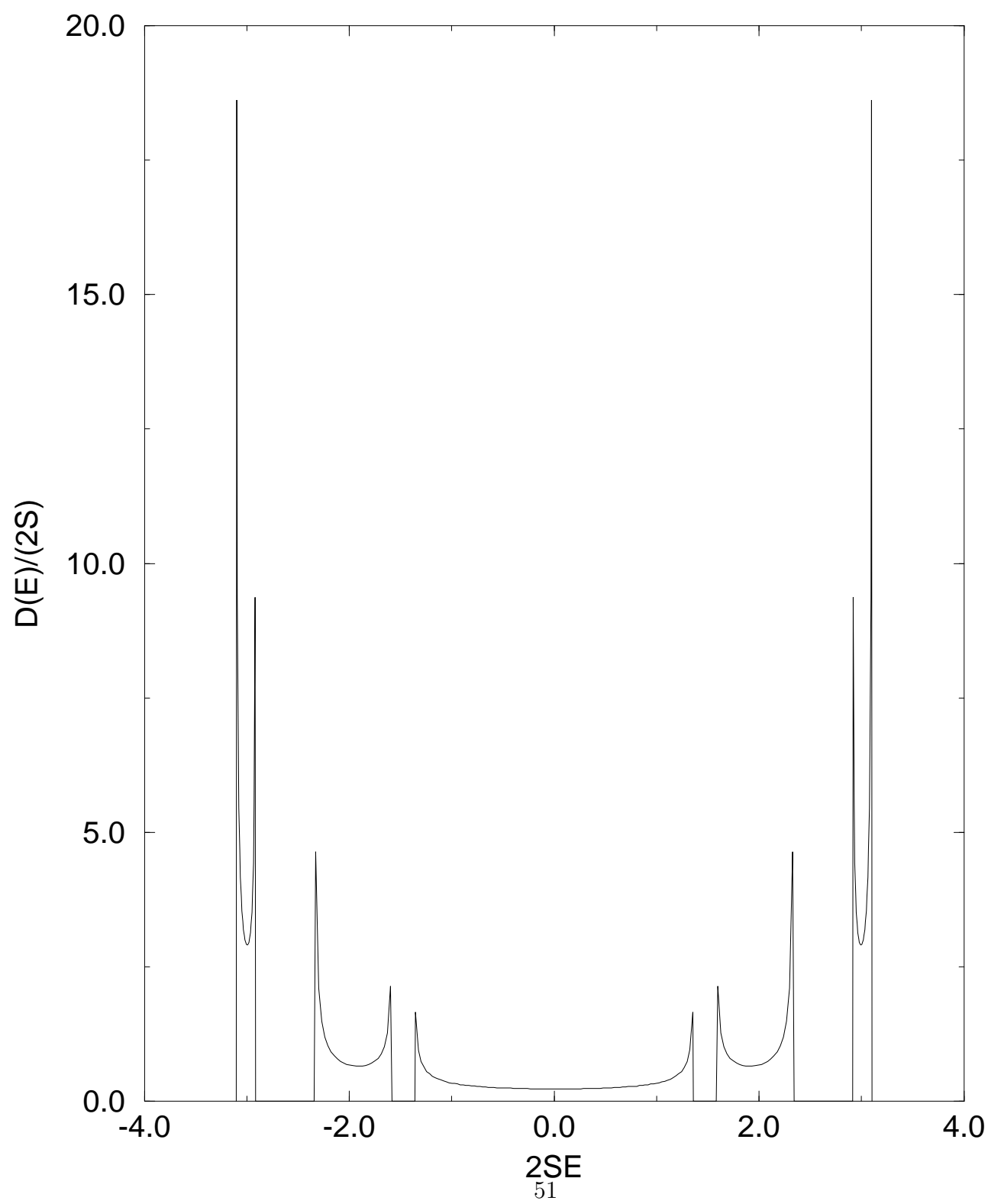
0 1 2 $n-1$ n $n+1$ $n+2$ $L+1$

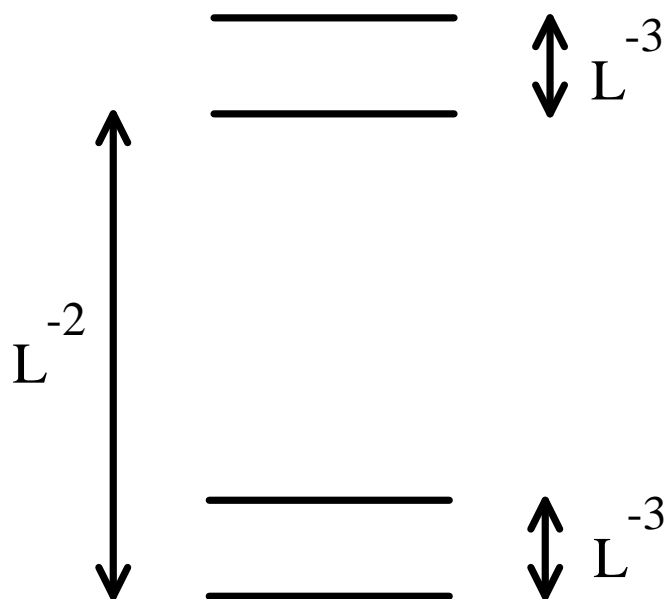




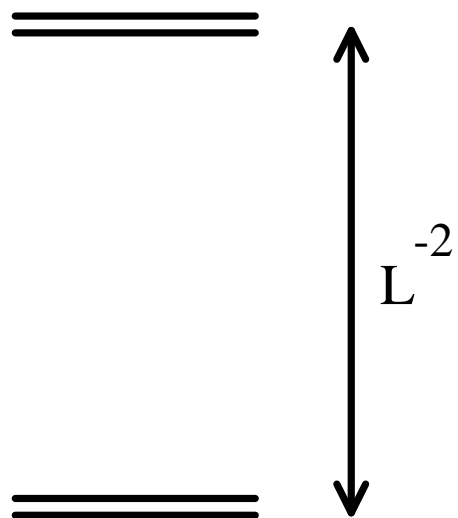








a) L even



b) L odd

